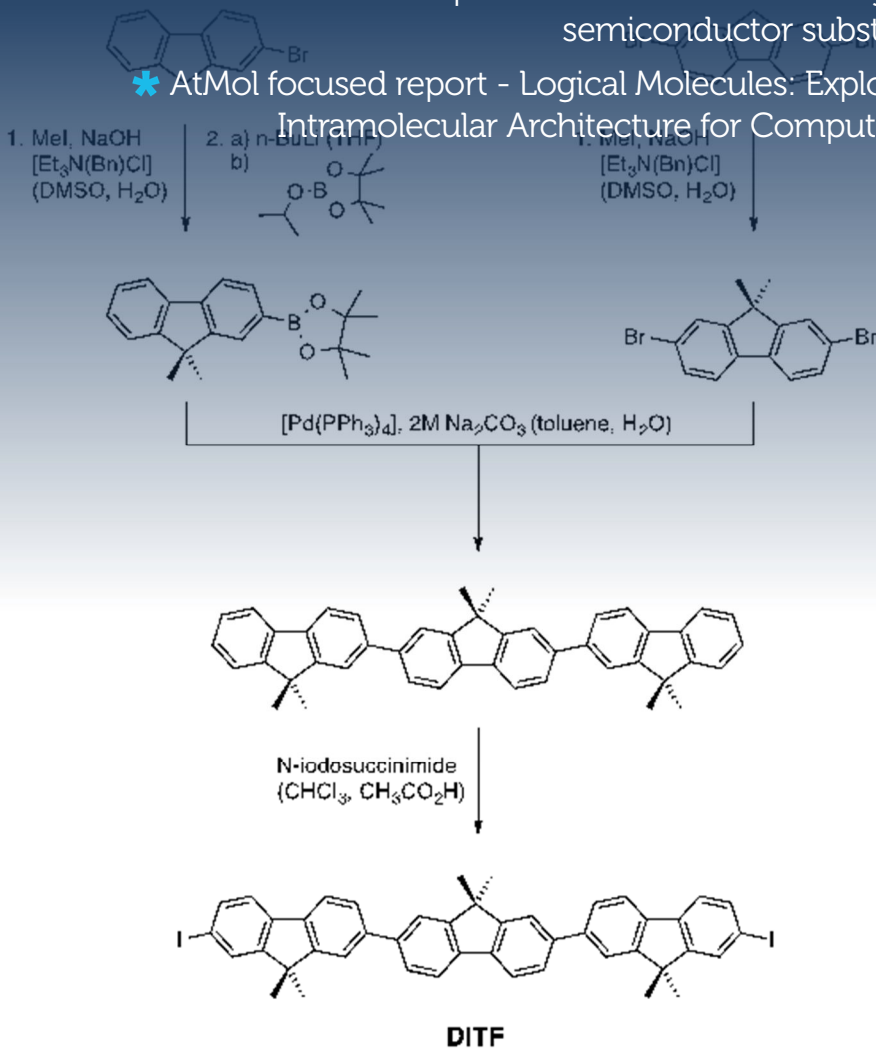




* Construction and characterization of atomic scale Quantum Hamiltonian Boolean logic gates on hydrogen passivated Si(100)

* On-surface polymerization as a facile method for bottom-up nanoconstruction on inorganic semiconductor substrates

* AtMol focused report - Logical Molecules: Exploiting Intramolecular Architecture for Computation



NANO GUNE EXTERNAL SERVICES

www.nanogune.eu/services/external

WE
CAN HELP YOU
TO LOOK FOR A
SOLUTION
TO YOUR PROBLEMS

CIC nanoGUNE offers **external services** to both academic and industrial users under a self-service mode or with the assistance of nanoGUNE specialists.

We open our advanced-microscopy laboratory, cleanroom, and various laboratories with nanomanufacturing and characterization equipment that guarantee optimum environmental conditions for developing nanotechnology.

MAKE A REQUEST TO
external.services@nanogune.eu



CIC nanoGUNE
Tolosa Hiribidea, 76
E-20018 Donostia - San Sebastian
+34 943 574 000

dear readers,

Dear Readers,

The AtMol Integrated Project (EU/ICT/FET) is currently establishing a comprehensive process flow for fabricating a molecular chip, i.e. a molecular processing unit comprising a single molecule connected to external mesoscopic electrodes with atomic scale precision and preserving the integrity of the gates down to the atomic level after the encapsulation.

This E-nano Newsletter special issue contains two articles and a focused report providing new insights on this hot research topic in Europe, in particular for the fabrication of future generations of electronic circuits with components miniaturized down to atomic scale.

Detailed information about the project, further reading documents and AtMol workshop series contributions could be found at www.atmol.eu.

We would like to thank all the authors who contributed to this issue as well as the European Commission for the financial support (ICT/FET FP7 AtMol project no. 270028).

> **Dr. Antonio Correia** Editor - Phantoms Foundation

contents

05 > nanoresearch - AtMol. Construction and characterization of atomic scale Quantum Hamiltonian Boolean logic gates on hydrogen passivated Si(100) /// M. Kolmer, R. Zuzak, S. Godlewski, G. Dridi, C. Joachim and M. Szymanski

09 > nanoresearch - AtMol. On-surface polymerization as a facile method for bottom-up nanoconstruction on inorganic semiconductor substrates /// M. Kolmer, R. Zuzak, A. A. Zebari, S. Godlewski, J. S. Prazdner-Bechcicki, M. Szymanski, W. Piskorz, F. Zasada, Z. Sojka, D. Bléger and S. Hecht

13 > AtMol publications. Further reading

15 > nanoresearch - AtMol focused report. Logical Molecules: Exploiting Intramolecular Architecture for Computation /// P. Moriarty and C. Joachim

editorial information

No. 31 December 2014. Published by Phantoms Foundation (Spain)

editor > Antonio Correia > antonio@phantomsnet.net

assistant editors > Maite Fernández, Conchi Narros and José Luis Roldán.

1500 copies of this issue have been printed. Full color newsletter available at:

www.phantomsnet.net/Foundation/newsletter.php

For any question please contact the editor at: antonio@phantomsnet.net

editorial board > Adriana Gil (Spain), Christian Joachim (CEMES-CNRS, France), Ron Reifenger (Purdue University, USA), Stephan Roche (ICN2, Spain), Juan José Sáenz (UAM, Spain), Pedro A. Serena (ICMM-CSIC, Spain), Didier Tonneau (CNRS-CINaM Université de la Méditerranée, France) and Rainer Waser (Research Center Jülich, Germany).

deadline for manuscript submission

Issue No. 32: March 31, 2015

Issue No. 33: May 31, 2015

depósito legal

legal deposit

BI-2194/2011

printing

Gráficas

Indauchu

www.atmol.eu

Atomic Scale and Single Molecule Logic Gate Technologies

*Atom by atom constructed dimer dangling
bond wire on an Si(100)H surface*



Construction and characterization of atomic scale Quantum Hamiltonian Boolean logic gates on hydrogen passivated Si(100)

Marek Kolmer¹, Rafal Zuzak¹, Szymon Godlewski¹, Ghassen Dridi², Christian Joachim² and Marek Szymonski¹

¹ Centre for Nanometer-Scale Science and Advanced Materials, NANOSAM, Faculty of Physics, Astronomy and Applied Computer Science, Jagiellonian University, Kraków, Poland
² Nanosciences Group & MANA Satellite, CEMES-CNRS, Toulouse, France

Introduction

A Quantum Hamiltonian Computing (QHC) Boolean logic approach is based on the control of the intrinsic time dependent evolution of a well designed quantum system by the logical inputs. In a quantum system of a surface dangling bond (DB) network prepared in a non-stationary initial state $|\psi(0)\rangle$, the time evolution is described by the time dependent state vector $|\psi(t)\rangle = e^{-iHt/\hbar} |\psi(0)\rangle$, where H is the Hamiltonian of the quantum system [1]. Any arithmetic or logic operations performed by this quantum system can be interpreted as a $|\psi(t)\rangle \leftarrow |\psi(0)\rangle$ trajectory

control on its quantum state space. The electronic structure of the gate, i.e. the H matrix elements, depend on the practical way chosen to encode the logical inputs and to measure the logical outputs of the gate. In AtMol project, we are encoding the $\{\alpha_1 \dots, \alpha_i \dots, \alpha_k\}$ digital input in the Hamiltonian $H = H(\alpha_1 \dots, \alpha_i \dots, \alpha_k)$, while the $\{\beta_1 \dots, \beta_i \dots, \beta_k\}$ digital output words are probed on well selected target states.

In the practical approach, we had explored recently how to design a robust QHC DB surface logic gates using the symmetry and the DB states available on a Si(100)H surface. Such gates can be easily implemented on this surface by extracting 2 DBs from the same dimer on the same row to create 2 quantum states required per node. This leads to the surface structure construction presented in Figure 1, where the logical input encoding have been chosen by attributing a logical "0" when there are no H atoms within a dimer and a logical "1", if the 2 H atoms are saturating the 2 Si

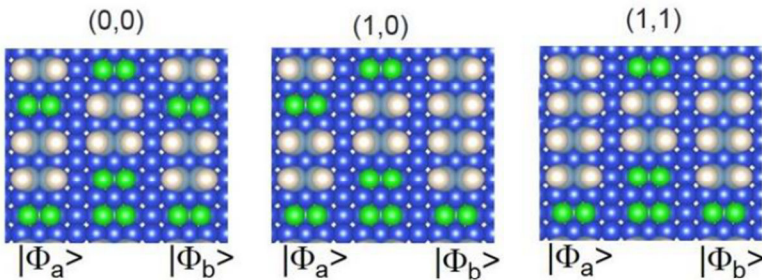


Fig. 1 > Schematic representation of QHC NOR/OR Boolean logic gate implemented on the Si(001):H by extracting DB dimers from the neighboring hydrogen rows./

surface atoms on the same dimer. In addition, a top DB dimer is added to reinforce the electronic interactions between the input and the core of the QHC gate. This leads to a 12×12 QHC simplified tight binding matrix which is performing like a NOR, XOR or AND Boolean logic gates depending on the values of the matrix structural parameters.

Experimental details

The practical construction of the selected QHC surface atomic circuits has been done following the appropriate scanning tunneling microscope (STM) tip-induced desorption protocols described in details elsewhere [2]. Atomically perfect surfaces were obtained either by in-situ ultra-high vacuum (UHV) de-bonding of SiHx bonded wafers provided by CEAL-LETI, Grenoble [2], or by standard UHV surface preparation including cycles of direct current heating followed by surface hydrogenation. The construction of individual DB involves a few steps: at first, the STM tip is positioned over the H atom selected for extraction in a filled-state constant current mode imaging. Then the feedback loop is switched off and the voltage is reversed and raised into the range of 2,5V-3,5V which allows desorption of an individual H atom. This is recorded in a current versus time

single as a sudden change of the tunneling current within several hundreds of milliseconds as shown in Fig. 2A. The above described procedure provides a single DB on surface. DB dimers are obtained by repetition of the procedure with the tip positioned over the neighboring H atom. The procedure is visualized in Fig. 2B-2E, where single DBs and DB dimers are shown. With the use of this protocol, DB lines and small circuits can be constructed atom by atom on a Si(001):H surface with the desired complexity.

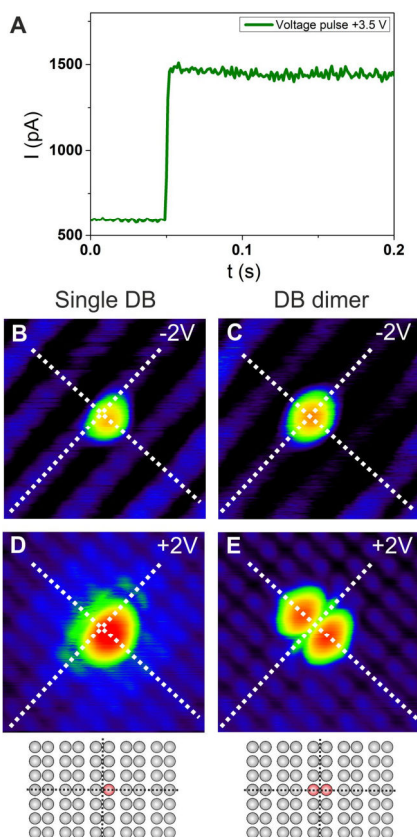


Fig. 2 > A) $I(t)$ characteristics recorded during the LT-UHV-STM tip induced desorption of a single H atom from Si(001)-(2x1):H. The voltage pulse applied on the tip was +3.5 V with respect to the sample. **B-E)** Filled state (B,C) and empty state (D,E) state STM images of the same 3.5 nm x 3.5 nm surface area presenting single (B,D) and double (C,E) DBs, which are the result of consecutive STM tip induced hydrogen atom desorption. STM scanning parameters: 10 pA, -2 V for filled state and 10 pA, +2 V for empty state imaging. Structural models of presented structures are also shown. Grey and red circles depict hydrogenated and bare silicon atoms respectively. Dashed lines on STM scans and models are placed for clarifying positions of atoms. Reproduced with permission from [2]./

A single DB was observed in both filled and empty state STM images as a protrusion, located asymmetrically with respect to the reconstruction row of Si(001):H, as shown in Fig. 2B and Fig. 2D. Desorption of the second hydrogen atom from the Si dimer led to formation of an isolated DB dimer. This structure filled and empty state STM images are shown in Fig. 2C and Fig. 2E, respectively. In both cases symmetric protrusion for moderate imaging conditions (10 pA current, -2 V and +2 V biases) are recorded. It shows a characteristic “butterfly” contrast in the empty state image. These observations are in agreement with previous STM measurements performed at RT [3], 80 K [4] and 5 K [5].

Results

Extraction of hydrogen atoms from neighboring hydrogenated silicon dimers induces coupling between the already constructed DBs. The coupling varies with the DB structure orientation, which can be taken as an advantage for the design and construction of atomic scale logic gates [6-8]. The interactions between neighboring DB dimers are expected to stabilize the buckled dimer configuration, as already observed for bare reconstructed silicon surface [9] and for short DB dimer lines formed on Ge(001):H surface [6,10]. However, this was not the case for the short DB dimer structures as presented in Figure 3.

Two DB dimers oriented along (Fig.3 A,C) and across (Fig.3 B,D) the reconstruction rows did not show a buckling and appeared symmetric at both bias polarizations. The characteristic empty state contrast of a single isolated DB dimer evolved towards a four-lobe and a three-lobe structures for parallel (Fig.3 C,E) and perpendicular (Fig.3 D,F)

geometries, respectively. Note that, due to the weak interaction between DBs, central maxima of two perpendicularly oriented DB dimer structures appear brighter in Fig.3D empty state STM image, what is clearly demonstrated by corresponding STM height profile (Fig. 3F).

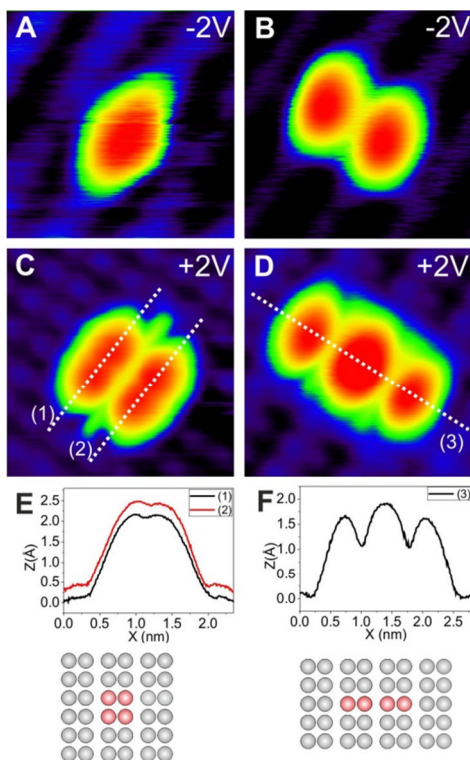


Fig. 3 > A-D Filled state (A,B) and empty state (C,D) STM images of Si(100) :H 2.5 nm × 2.5 nm surface area presenting short lines of two DB dimers, which are oriented along (A,C) and across (B,D) reconstruction rows. STM scanning parameters: 10 pA, -2 V for filled state and 10 pA, +2 V for empty state imaging. (E,F) Height profiles taken from the STM images C and D. Structural models of presented structures are also shown. Grey and red circles depict hydrogenated and bare silicon atoms respectively. Reproduced with permission from [2]./

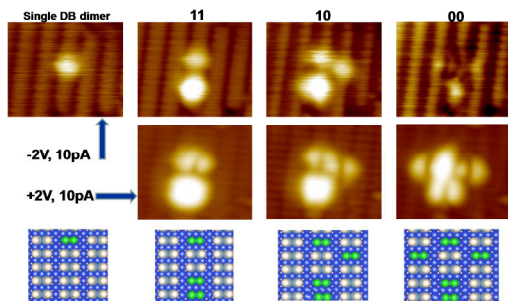


Fig. 4 > Construction of a dangling bond NOR logic gate on an Si(100)-(2x1)-H surface. The logical inputs for the different structures of the gate are given above the STM images. STM imaging parameters are -2V, 10 pA (**upper row**) and +2V, 10 pA (**lower row**). The NOR gate was optimized for a planar metallic nano-pad output surface measurements. (a) the reference STM image to certify that the 2 H were extracted from the same dimer row on the Si(100)H./

Next and following the QHC design of a NOR gate, we have constructed a complete QHC NOR gate on the Si(100)H surface. STM-based extraction of H atoms to fabricate NOR gate has been performed on slightly doped H:Si(100) sample (p-type B doping) kept at liquid nitrogen (77K) temperature using Krakow's UHV LT STM system. The resulting DB structures are shown in Figure 4. It is striking that a change of the input from "00" to "11" causes a dramatic modification of the dangling bond structure appearance for both filled and empty states. Note that DB dimers are buckled in "00" gate structure for -2V at 77K. Such a buckling was not observed for the structures constructed in our previous work even at liquid helium temperature [2].

In conclusion, we have demonstrated that a construction of prototypical QHC Boolean logic gates on hydrogen passivated Si(100):H was feasible and the gate atomic scale structure was characterized by high resolution UHV-STM imaging.

References

- [1] H. Kawai, F. Ample, Q. Wang, Y.K. Yeo, M. Saeys, C. Joachim, Dangling-bond logic gates on a Si(100)-(2 × 1)-H surface, *Journal of Physics: Condensed Matter* 24 (2012) 095011.
- [2] M. Kolmer, S. Godlewski, R. Zuzak, M. Wojtaszek, C. Rauer, A. Thuairé, J.-M. Hartmann, H. Moriceau, C. Joachim, M. Szymonski, Atomic scale fabrication of dangling bond structures on hydrogen passivated Si(001) wafers processed and nanopackaged in a clean room environment, *Applied Surface Science* 288 (2014) 83-89.
- [3] J.J. Boland, Evidence of pairing and its role in the recombinative desorption of hydrogen from the Si(100)-2×1 surface, *Physical Review Letters* 67 (1991) 1539–1542.
- [4] D. Chen, J. Boland, Chemisorption-induced disruption of surface electronic structure: Hydrogen adsorption on the Si(100)-2×1 surface, *Physical Review B* 65 (2002) 165336.
- [5] A. Bellec, D. Riedel, G. Dujardin, O. Boudrioua, L. Chaput, L. Stauffer, P. Sonnet, Electronic properties of the n-doped hydrogenated silicon (100) surface and dehydrogenated structures at 5 K, *Physical Review B* 80 (2009) 245434.
- [6] M. Kolmer, S. Godlewski, H. Kawai, B. Such, F. Krok, M. Saeys, C. Joachim, M. Szymonski, Electronic properties of STM-constructed dangling-bond dimer lines on a Ge(001)-(2×1):H surface, *Physical Review B* 86 (2012) 125307.
- [7] C. Joachim, D. Martrou, M. Rezeq, C. Troadec, D. Jie, N. Chandrasekhar, S. Gauthier, Multiple atomic scale solid surface interconnects for atom circuits and molecule logic gates, *Journal of Physics: Condensed Matter* 22 (2010) 084025.
- [8] J.S. Prauzner-Bechcicki, S. Godlewski, M. Szymonski, Atomic- and molecular-scale devices and systems for single-molecule electronics, *Physica Status Solidi (a)* 209 (2012) 603–613.
- [9] R.A. Wolkow, Direct Observation of an Increase in Buckled Dimers on Si(001) at Low Temperature, *Physical Review Letters* 68 (1992) 2636–2639
- [10] M. Kolmer, S. Godlewski, J. Lis, B. Such, L. Kantorovich, M. Szymonski, Construction of atomic-scale logic gates on a surface of hydrogen passivated germanium, *Microelectronic Engineering* 109 (2013) 262-265.

On-surface polymerization as a facile method for bottom-up nanoconstruction on inorganic semiconductor substrates

Marek Kolmer¹, Rafal Zuzak¹, Amir A. Zebari¹, Szymon Godlewski¹, Jakub S. Prauzner-Bechcicki¹, Marek Szymonski¹, Witold Piskorz², Filip Zasada², Zbigniew Sojka², David Bléger³ and Stefan Hecht³

¹ Centre for Nanometer-Scale Science and Advanced Materials, NANOSAM, Faculty of Physics, Astronomy and Applied Computer Science, Jagiellonian University, Kraków, Poland

² Faculty of Chemistry, Jagiellonian University, Krakow, Poland

³ Department of Chemistry, Humboldt-Universität zu Berlin, Berlin, Germany

Over the past years on-surface polymerization, enabling direct connection of a variety of suitable monomer building blocks directly on a given substrate, has emerged as a vibrant field of research. A potpourri of linking reactions giving rise to a large structural and compositional diversity of the prepared 1D and 2D polymer has been explored thus far yet on a limited number of substrates, primarily coinage metal surfaces. This is primarily due to STM analysis used in most investigations as it is greatly facilitated on these noble metal surfaces. Only recently on-surface linking reactions have been carried out successfully on inorganic insulator and, perhaps more appealing, on inorganic semiconductor substrates. Here, we highlight our most recent findings of polymerizing organic monomers via aryl-aryl coupling step-growth in-situ on a particular rutile (TiO₂) surface. We show monomer synthesis, provide evidence for successful on-surface polymerization, and explore crucial reaction parameters. Our findings significantly enhance the scope of our on-surface polymerization method and illustrate its tremendous potential for the bottom-up generation of organic-inorganic hybrid nanostructures.

The bottom-up generation of covalent nanostructures directly on substrate surfaces via the so called “on-surface polymerization” approach, pioneered by us [1], has recently become a very active field in nanoscience. A large variety of well-defined nanostructures including molecular wires [2-4], 2D molecular networks [5-7], or confined graphene nanostructures [8-10] has been generated from suitable

monomers. These precursor molecules possess specific linking sites, which are activated after their deposition on a substrate surface, typically coinage metals (Cu, Ag, and Au). While the noble metal surface facilitates analysis via STM imaging, it also catalyzes activation of the aryl halide monomers as well as coupling of the formed aryl intermediates. However, in particular in the case of preparing π -conjugated polymers on top of the metallic surface their optoelectronic functions are largely sacrificed and hence from the standpoint of practical applications of on-surface covalent coupling, highly ordered semiconducting [11] or insulating [3, 10, 12] surfaces clearly represent much more attractive platforms. In particular inorganic semiconductor surfaces, such as transition metal oxides, present a complementary match for the organic semiconductors formed via on-surface polymerization and offer advantageous optical as well as photo- and electrochemical properties. These properties could potentially be enhanced by an on-surface polymerized organic semiconductor layer and hence resulting in possible applications in photonics, photocatalysis or gas and bio sensing [13, 15]. In this context, titanium dioxide constitutes a privileged inorganic semiconductor, which has attracted lots of attention in the context of dye-sensitized solar cells and photocatalytic water splitting and waste-water detoxification. From a surface science perspective in particular the surface of rutile TiO₂ (011) has been intensely investigated recently [16,17].

For the first time we could recently demonstrate the feasibility of the on-surface covalent coupling of aryl halide

precursors on the rutile $\text{TiO}_2(011)-(2 \times 1)$ surface (Figure 1) [11]. By depositing 10,10-dibromo-9,9'-bianthryl (DBBA) monomers on a $\text{TiO}_2(011)-(2 \times 1)$ surface kept at 270 °C growth of oligomers reaching up to 10 nm chain length and corresponding to ca. 20-mers was observed. In contrast to the process consisting of polymerization followed by intramolecular annulation on Au(111) [8], the latter cyclodehydrogenation reaction could not be induced on the $\text{TiO}_2(011)-(2 \times 1)$ surface leading to formation of polyanthrylene and not narrow armchair-type graphene nanoribbons. However, the successful covalent coupling of aryl halides on the $\text{TiO}_2(011)-(2 \times 1)$ surface was encouraging and motivated us to investigate critical parameters in the polymerization process on such non-metallic substrate. In particular, the specifics of the surface, such as reconstruction, redox state of the titanium atoms, and presence of hydroxyl groups was in the focus of our investigations as they represent a major difference to the coinage metals and should strongly affect the operating polymerization mechanism. Furthermore, the monomer was changed to potentially lower the temperature necessary to induce polymerization.

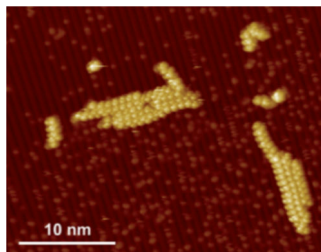
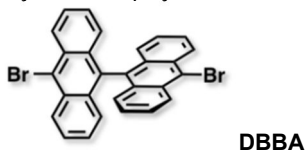


Fig. 1 > Initial polymerization of 10,10'-dibromo-9,9'-bianthryl (DBBA) monomers on $\text{TiO}_2(011)$ [11]./

On the one hand an oligofluorene monomer building block as a well-studied repeating unit in on-surface polymerization [2-4] was equipped with terminal iodine substituents as they were expected to further lower the necessary activation temperature [5]. For this purpose, diiodoterfluorene (DITF) was prepared (Figure 2). Synthesis involves preparation of 9,9-dimethylated terminal fluorenes, which as boronic esters are being coupled to a 2,7-dibromo-9,9-dimethylfluorene core yielding the barely soluble permethylated terfluorene (TF), which is iodinated in the final step of the synthesis.

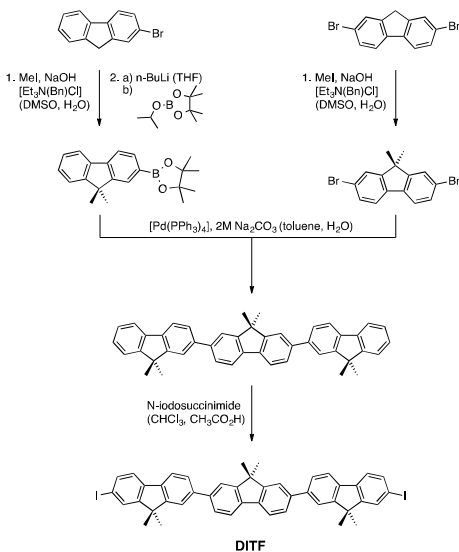


Fig. 2 > Synthesis of diiodoterfluorene (DITF) monomers./

On the other hand, reduced $r\text{-TiO}_2(011)-(2 \times 1)$ surfaces containing various amounts of surface hydroxyl groups were prepared. The (2×1) reconstruction of $\text{TiO}_2(011)$ consists of two-fold coordinated terminal oxygen and five-fold coordinated terminal titanium atoms forming a characteristic zigzag pattern on the rows running along the [01-1]

direction [18]. Hydrogen atom adsorption on the terminal exposed oxygen atoms leads to formation of surface hydroxyl groups [19]. In scanning tunneling microscopy (STM) images these surface hydroxyl groups are observed as bright protrusions located nonsymmetrically on top of the zigzag pattern. Mechanistically, the presence of surface hydroxyl groups should have a dramatic effect on the coupling mechanism as it is assumed to proceed via a surface stabilized aryl radical on coinage metal surfaces. Therefore, one would at first expect hydroxyl groups to possibly terminate polymerization by hydrogen atom abstraction from the outcome of the on-surface polymerization a $r\text{-TiO}_2(011)\text{-}(2\times 1)$ surface containing less than 0.5% coverage of hydroxyl groups was prepared [17]. Note that the coverage is given relative to the maximum number of available two-fold coordinated terminal oxygen atoms. For comparison, two other types of well-defined $r\text{-TiO}_2(011)\text{-}(2\times 1)$ surfaces with medium ($5 \pm 1\%$) and high ($20 \pm 1\%$) hydroxyl group coverage were prepared using atomic hydrogen to react with the $r\text{-TiO}_2(011)\text{-}(2\times 1)$ surface.

Polymerization of the DITF monomers was carried out by evaporation on the differently prepared substrates kept at 260°C . STM analysis of the product mixture on the $r\text{-TiO}_2(011)$ surface as well as an oxidized $o\text{-TiO}_2(011)$ surface revealed that no polymerization took place. This is rather surprising as both surfaces practically do not contain surface hydroxyl groups and hence formed aryl radicals (if formed) should have the opportunity to dimerize, i.e. connect, without termination. On the contrary, upon evaporation of DITF monomers on the two medium and highly hydroxylated $r\text{-TiO}_2(011)$ surfaces leads to formation of polymers (Figure 3),

which adsorb along the surface reconstruction rows. High-resolution STM imaging clearly revealed the bright protrusions of the methyl groups for each fluorene unit and analysis of the observed distances proved covalent connection into polyfluorene chains as previously observed only on coinage metal surfaces [2-4].

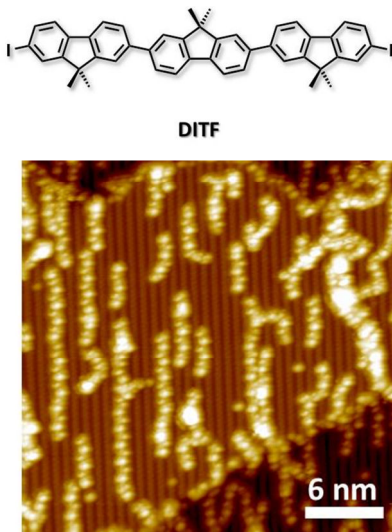


Fig. 3 > Polymerization of diiodoterfluorene (DITF) monomers on a reduced $r\text{-TiO}_2(011)\text{-}(2\times 1)$ surface with medium ($5 \pm 1\%$) hydroxyl group coverage at 260°C .

Interestingly, when comparing STM images before and after polymerization it appears that the surface hydroxyl groups are consumed during the polymerization process. The disappearance of the surface hydroxyl groups must be due linked to the operating polymerization mechanism (or a chemical reaction connected to it) because treating the rutile $\text{TiO}_2(011)\text{-}(2\times 1)$ at these temperatures typically does not lead to desorption of the surface-bound hydrogen atoms [19]. One possible explanation might be trapping of the formed iodine substituents as gaseous H-I. Importantly, polymerizations carried

out on the medium hydroxylated surface yield longer polymer chains as compared to the ones carried out on the highly hydroxylated substrate as revealed from STM image analysis and detailed statistics. Therefore, it seems that there is an optimum coverage of surface hydroxyl groups. It should be emphasized here that defects such terrace edges or domain boundaries act as anchoring sites for the formed oligomers and hence reducing their number should lead to further increase of the polymerization efficiency.

In conclusion, we have experimentally demonstrated the feasibility and generality of on-surface polymerization on partially hydroxylated $r\text{-TiO}_2(011)$ surfaces and investigated critical growth parameters. Based on our experimental findings, a detailed mechanistic rationale is currently being developed. From a more applied perspective our approach should now be applied to grow a large variety of oligomers and polymers on various transition metal oxides and other inorganic semiconductors thereby leading to interesting hybrid systems with matched valence and conduction bands of both organic and inorganic semiconductors.

Acknowledgements

Generous support by European Project "AtMol" is gratefully acknowledged.

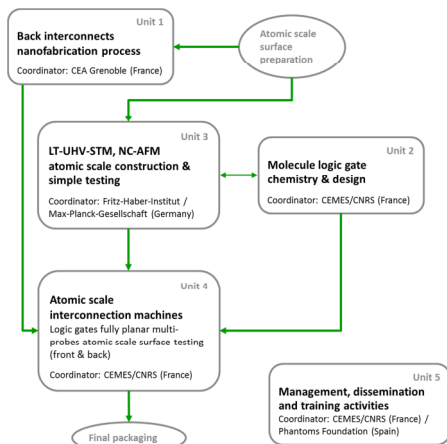
References

- Grill, L.; Dyer, M.; Lafferentz, L.; Persson, M.; Peters, M. V.; Hecht, S. *Nat. Nanotechnol.* **2**, 687 (2007).
- Lafferentz, L.; Ample, F.; Yu, H.; Hecht, S.; Joachim, C.; Grill, L. *Science* **323**, 1193 (2009).
- Bombis, C.; Ample, F.; Lafferentz, L.; Yu, H.; Hecht, S.; Joachim, C.; Grill, L. *Angew. Chem. Int. Ed.* **48**, 9966 (2009).
- Kawai, S.; Koch, M.; Gnecco, E.; Sadeghi, A.; Pawlak, R.; Glatzel, T.; Schwarz, J.; Goedecker, S.; Hecht, S.; Baratoff, A.; Grill, L.; Meyer, E. *Proc. Nat. Acad. Sci.* **111**, 3968 (2014).
- Lafferentz, L.; Eberhardt, V.; Dri, C.; Africh, C.; Comelli, G.; Esch, F.; Hecht, S.; Grill, L. *Nat. Chem.* **4**, 215 (2012).
- Bieri, M.; Nguyen, M. T.; Groning, O.; Cai, J. M.; Treier, M.; Ait-Mansour, K.; Ruffieux, P.; Pignedoli, C. A.; Passerone, D.; Kastler, M.; Mullen, K.; Fasel, R. *J. Am. Chem. Soc.* **132**, 16669 (2010).
- Eichhorn, J.; Nieckarz, D.; Ochs, O.; Samanta, D.; Schmittl, M.; Szabelski, P. J.; Lackinger, M. *ACS Nano* **8**, 7880 (2014).
- Cai, J.; Ruffieux, P.; Jaafar, R.; Bieri, M.; Braun, T.; Blankenburg, S.; Muoth, M.; Seitsonen, A. P.; Saleh, M.; Feng, X.; Müllen, K.; Fasel, R. *Nature* **466**, 470 (2010).
- Koch, M.; Ample, F.; Joachim, C.; Grill, L. *Nat. Nanotechnol.* **7**, 713 (2012).
- Palma, C. A.; Diller, K.; Berger, R.; Welle, A.; Bjork, J.; Cabellos, J. L.; Mowbray, D. J.; Papageorgiou, A. C.; Ileva, N. P.; Matich, S.; Margapoti, E.; Niessner, R.; Menges, B.; Reichert, J.; Feng, X. L.; Rader, H. J.; Klappenberger, F.; Rubio, A.; Mullen, K.; Barth, J. V. *J. Am. Chem. Soc.* **136**, 4651 (2014).
- Kolmer, M.; Ahmad Zebari, A. A.; Prauzner-Bechcicki, J. S.; Piskorz, W.; Zasada, F.; Godlewski, S.; Such, B.; Sojka, Z.; Szymonski, M. *Angew. Chem. Int. Ed.* **52**, 10300 (2013).
- Kittelmann, M.; Nimrich, M.; Lindner, R.; Gourdon, A.; Kuhnle, A. *ACS Nano* **7**, 5614 (2013).
- Diebold, U. *Surf. Sci. Rep.* **48**, 53 (2003).
- Pang, C. L.; Lindsay, R.; Thornton, G. *Chem. Rev.* **113**, 3887 (2013).
- Henderson, M. A. *Surf. Sci. Rep.* **66**, 185 (2011).
- Tao, J.; Luttrell, T.; Batzill, M. *Nat. Chem.* **3**, 296 (2011).
- Addou, R.; Senftle, T. P.; O'Connor, N.; Janik, M. J.; van Duin, A. C. T.; Batzill, M. *ACS Nano* **8**, 6321 (2014).
- Woolcot, T.; Teobaldi, G.; Pang, C. L.; Beglitis, N. S.; Fisher, A. J.; Hofer, W. A.; Thornton, G. *Phys. Rev. Lett.* **109**, 156105 (2012).
- Tao, J.; Cuan, Q.; Gong, X.-Q.; Batzill, M. *J. Phys. Chem. C* **116**, 20438 (2012).



Cover Image:

Synthesis of diiododotterfluorene (DITF) monomers // M. Kolmer, R. Zuzak, A. A. Zebari, S. Godlewski, J. S. Prauzner-Bechcicki, M. Szymonski, W. Piskorz, F. Zasada, Z. Sojka, D. Bléger and S. Hecht



- Quantifying the atomic-level mechanics of single long physisorbed molecular chains; PNAS March 18, (2014) vol. 111 no. 11 3968–3972
- Gold(I) Carbenes by Retro-Buchner Reaction: Generation and Fate; J. Am. Chem. Soc. (2014), 136, 801–809
- Spin transport in dangling-bond wires on doped H-passivated Si(100); IOP Publishing Nanotechnology 25 (2014) 465703 (6pp)
- Inversion layer on the Ge(001) surface from the four-probe conductance measurements; Appl. Phys. Lett. 105 (2014) 042111
- Hole-Electron Quantum Tunnelling Interferences through a Molecular Junction; Chem. Phys. Lett., 592, 272 (2014)
- Surface Creation of Nanojunction Between fullerene and 1D conductive polymers; ACS Nano, 8, 12259 (2014)
- One way rotation and efficiency of a single molecule motor driven by a shot noise; Nanoscale, 6, 2793 (2014)
- Quantum coherence of bulk electrons on metals revealed by scanning tunneling spectroscopy; Phys. Rev. B 89, 205433 (2014)
- Intermolecular Reactions of Gold(I)-Carbenes with Furans by Related Mechanisms; Org. Chem. Front. 1, 759–764 (2014)
- Formal (4+1) Cycloaddition of Methylcyclopropanes with 7-aryl-1,3,5-cycloheptatrienes via Triple Gold(I)-Catalysis; Angew. Chem. Int. Ed. 53, 14022–14026 (2014)
- Controlling intramolecular hydrogen transfer in a porphycene molecule with single atoms or molecules located nearby; Nature Chemistry Vol 6 January (2014)
- Adatoms Underneath Single Porphyrin Molecules on Au(111); Journal of the American Chemical Society, DOI: 10.1021/ja510528x
- Surface-Assisted Reactions toward Formation of Graphene Nanoribbons on Au(110) Surface; Journal of Physical Chemistry C, DOI: 10.1021/jp509415r
- Substrate-controlled linking of molecular building blocks: Au(111) vs. Cu(111); Surface Science 627 (2014) 70–74
- Driving Molecular Machines Using the Tip of a Scanning Tunnelling Microscope; Springer Series: Advances in Atom and Single Molecule Machine; Vol. V, p. 187 (2015). ISBN 978-3-319-13871-8
- Si(100) 2x1 H dimer rows contrast inversion in low temperature scanning tunneling microscope images; Surf. Sci. Lett., 632, L13 (2015)
- Molecular versus Atomic scale circuits for Boolean logic gates (and more) at the atomic scale; E-Nano Newsletter (Issue 29) 2014, pages 29-31
- Experimental approach towards molecular circuits; E-Nano Newsletter (Issue 29) 2014, pages 32-35
- Surface atomic wires for interconnects and logic gate design; E-Nano Newsletter (Issue 29) 2014, pages 37-42



New

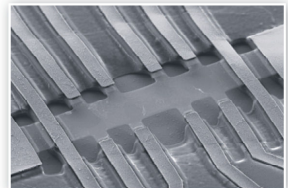
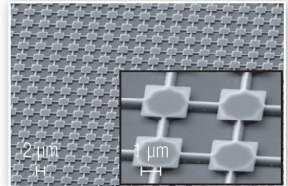
PIONEER Two

Best of both worlds:
Direct write and direct view

The ideal Nanolithography-SEM hybrid at an affordable price

- The world's smallest beam size in a professional electron beam lithography system
- Sub 8 nm linewidth guarantee
- Analytical capabilities for material and life science (SEM, EDX, material contrast...)

www.raith.com



MULTI TECHNIQUE ELECTRON BEAM LITHOGRAPHY

RAITH
NANOFABRICATION

Logical Molecules: Exploiting Intramolecular Architecture for Computation

Philip Moriarty¹ and Christian Joachim²

¹ The School of Physics and Astronomy, The University of Nottingham, Nottingham NG7 2RD, UK
² CEMES/CNRS, 29 Rue J. Marvig, BP 94347, 31055 Toulouse Cedex, France

We outline, from an experimentalist's perspective, the key concepts underpinning quantum Hamiltonian computing (QHC), the distinction between QHC and quantum computing, and the design of intramolecular logic gates for information processing using the QHC approach. Our aim is to provide a short and readable overview that can be used as a "primer" for researchers who are new to the field. In addition, we summarise a number of the key advances made by the European Commission-funded AtMol consortium (www.atmol.eu) in the realisation of QHC prototypes, the development of dangling bond-mediated logic gates, and the strategies pursued to connect intramolecular processors to the macroscopic world.

I. From Classical To Quantum Logic

In 1974, in a pioneering, far-sighted, and immensely influential *gedankenexperiment*, Aviram and Ratner proposed that a single molecule could be used as an electronic component - a combination of a chemical donor, acceptor, and a spacer unit would, they claimed, act as a diode [1]. Their paper introduced the now-pervasive field of molecular electronics, and over the years since Aviram and Ratner's work was published, an impressive array of examples of single molecule transport have been realised in a variety of systems. A review of a significant amount of molecular electronics research (up until 2000) was co-authored by one of us (CJ) and remains an important and comprehensive introduction to very many of the key principles and advances in the field [2]. It is the final paragraph of that review, however, which sets the scene for what we shall discuss here:

Indeed, as synergistic and cooperative effects in complex molecular systems

are understood and controlled, new electronic devices based on unconventional operating principles might be developed. In short, it seems that applying conventional electronic concepts and approaches will not necessarily be the best way to achieve functional molecular devices operating on a dimensional scale where quantum mechanics dominates.

Our focus is on the embedding of logical operations within the architecture of a single molecule (or within ensembles of atomic orbitals that in many ways mimic molecular states). This was the primary rationale underpinning the multi-partner (and multi-million) EU-funded AtMol project, and this brief review will cover just how AtMol contributed to the development of the state of the art in monomolecular electronics/logic operations. Information processing via the manipulation of quantum states is therefore a central theme of our review, but, as we shall discuss in more detail below, there are major differences between the type of approach adopted in the so-called quantum Hamiltonian computing (QHC) method introduced by CJ [3] - a core aspect of the AtMol network's research - and the much broader field of quantum computing. Key amongst these is the treatment and exploitation of the phase of the wave function.

One particularly instructive and elegant way of introducing the central difference between the classical and quantum approaches to molecular circuitry, as adopted by CJ in a recent News and Views article [4], is to consider those fundamental principles of circuit design known as Kirchoff's laws, a mainstay of first year undergraduate physics and

engineering degree courses. The electronic conductance of a molecular junction depends, like any quantum system involving structures of comparable size to the electron coherence length, on the various paths (and path differences) that are present. As illustrated in Fig. 1, constructive interference of identical pathways (with individual conductances of G_1 and G_2 respectively) contributes an increase in conductance of $2\sqrt{G_1 G_2}$ above the classical value, $G_1 + G_2$, expected from Kirchoff's laws. When, however, the pathways are not identical – due to differences in the electron transit time, for example – then the phase relationship is 'scrambled' and the constructive interference term plays less of a role. In the limit of entirely independent electron transport pathways (Fig. 1(d)), the classical, i.e. Kirchoff's law, value of the conductance is recovered.

Vazquez et al [5] synthesized a number of molecules which were 'analogues' of the conduction pathway shown in Fig. 1(b) and measured the conductance of each of the molecules using a scanning tunneling microscope (STM)-actuated break-junction technique. They interpreted their conductance measurements in terms of conduction along either one, or two molecular "backbone" pathways, and argued that their data showed strong evidence of the contribution of quantum interference for molecules containing a double backbone (i.e. two phase coherent channels, as illustrated in Fig.1(b)).

In the AtMol project, however, the focus was on a very different strategy than a one-to-one mapping of the functionality of various elements of a circuit onto intramolecular topology. Our objective throughout was not to synthesise molecules whose structure was derived from spatially linking together smaller units which each had a given electronic functionality (e.g. wire, rectifier, node...). Instead, the aim was to embed logical

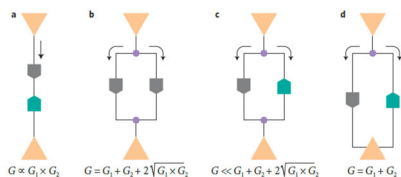


Fig. 1 > Schematic illustration of effects of intramolecular 'wiring' on total junction conductance, G , where G_1 and G_2 are the conductances of individual 'nodes' within a single molecule. The nodes are represented by the grey and green shapes, while the purple dots schematically illustrate the chemical groups within the molecule which determine current pathways within the molecule. **(a)** When the molecular nodes are wired in series, the conductance, G , is simply the product $G_1 G_2$. **(b)** If we add a second *identical* pathway through the molecule, and assuming no phase shift, the total conductance, G , is the sum of the individual node conductances and a term due to constructive interference of the conduction pathways, $G = G_1 + G_2 + 2\sqrt{G_1 G_2}$; **(c)** However, if the pathways are not identical then destructive interference will reduce the value of G ; **(d)** The process in (c) reaches its natural limit if there are independent connections to the molecule. This 'scrambles' the phase relationship between the pathways, eliminating the interference term, and reducing the total conductance to $G_1 + G_2$. Figure from ref [4]. ©Nature Publishing Group (2012)./

operations within the *Hamiltonian* of a given molecule (a strategy known as quantum Hamiltonian computing (QHC) which we discuss in detail below). This is a rather more "holistic" approach to molecular computing¹ which, while certainly a rather more challenging approach in terms of design principles, has the virtue of enabling, at least in principle, the realisation of logic operations in a rather more compact molecular design.

The quantum Hamiltonian protocol necessitates a very different approach to

¹There is often a danger in using the term "holistic" due to its connotations in alternative medicine and some of the more outlandish claims regarding quantum mechanics. Here we are using the term in its literal sense (and in the context of its original meaning): "characterized by the belief that the parts of something are intimately interconnected and explicable only by reference to the whole."

molecular computing. Instead of design principles based on intramolecular "topology" – in essence, the assumption that a circuit or gate should be based on the shape of a molecule – QHC forgoes traditional molecular electronics principles and translates logic operations directly to the quantum regime.

II. Quantum Hamiltonian Computing (QHC) vs Quantum Computing

It is important that we distinguish QHC from quantum computing (QC). Our aim, however, is not to give an exhaustive account of, or even an introduction to, quantum computing. The distinction between QHC and quantum computing can, however, be explained from rather basic principles, without the need to introduce an (unnecessarily) unwieldy mathematical formalism.

In any type of quantum calculation, the data are represented as quantum states which evolve and interact (in, of course, a non-classical process) to produce an output. The system evolves according to

$$|\psi(t)\rangle = e^{-\frac{iHt}{\hbar}} |\psi(0)\rangle \quad (1)$$

where $\psi(t)$ is the state of the system at time t , the initial state is $\psi(0)$, and H is the Hamiltonian of the system (which we assume is time-independent). In quantum computing, the system is prepared in a nonstationary state, $\psi(0)$, which evolves according to Eqn.1 above, and the output state is read at some time t . There are two key distinctions between classical and quantum computing: (i) quantum bits (now known ubiquitously as qubits) are not binary; they can exist in a superposition of states and so adopt any value consistent with the normalisation condition; and (ii) a quantum system, unlike its classical counterpart, can be prepared in an entangled state, where two (or, of course, more) qubits are not independent.

Entanglement is generally considered to be essential in order for quantum computing to surpass the capabilities of classical computers². Moreover, in QC, it is essential to protect the fragile quantum state from external influence, i.e. to avoid phase decoherence. (Alternatively, the computation needs to be carried out on a time scale sufficiently fast so that appreciable decoherence does not occur. This latter approach was adopted with some aplomb in a ground-breaking experiment by Walmsley and co-workers [7] which demonstrated the entanglement of macroscopic objects (diamond crystals).) Decoherence is just another manifestation of the type of phase scrambling which removed any quantum conductance behaviour from the molecular system shown in Fig. 1(d).

How then does QHC differ from QC? The clue is in the title of the technique. QHC involves manipulation of the Hamiltonian of the system – this is how a particular logic operation is encoded, and, correspondingly, H determines how input information is transformed to a particular output *at a given spatial position within the molecule*. QHC does not exploit qubits - it is the entire molecular quantum state that is exploited. This is a crucial distinction - temporal decoherence of the type that plagues quantum computing is no longer an issue because QHC does not require calculations to be carried out at a rate (much) faster than the decoherence time of a qubit. Indeed, QHC actively *exploits* decoherence – the system is repeatedly set up in a state $|\psi(0)\rangle$ (by sequential injection of electrons at a rate of $\sim 10^{10}$ Hz, i.e. a current ~ 1 nA) and the output is the time-averaged result of these preparation-relaxation events. The benefits with regard to decoherence are, however, offset by the requirement that reading the output of the QHC calculation necessitates

²...although, it must be stressed, non-entangled variants of QC are possible [6]

submolecular spatial resolution (as will become clear in the examples of intramolecular QHC logic outlined below). Fortunately, STM provides just the type of ultrahigh resolution that is necessary for QHC.

If the Hamiltonian effectively defines the Boolean truth table for the intramolecular gate (i.e. the relationship between the single bit inputs and out-puts), how then is information actually input into the molecule? There are two (inter-dependent) possibilities: the binary input can be encoded either via the Hamiltonian or via the initial state, $|\psi(0)\rangle$. These two strategies are inextricably coupled together, however. Using $|\psi(0)\rangle$ to encode the input data means that the Hamiltonian must take account of this initial state, and vice versa. This rather complicates the design of the molecular system but, as we'll show in the following section, this is certainly not an insurmountable problem.

III. Designing and Realising Intramolecular Logic Gates

Let's focus on one of the earliest examples of an intramolecular logic gate designed using the quantum Hamiltonian computing strategy (Fig. 2). This will ground the general theoretical principles in a specific system, and help to explain just how an intramolecular QHC logic gate is designed and implemented.

A decade ago, Duchemin and Joachim [8] showed how a half-adder logic function³ could be embedded within the Hamiltonian of a dinitro[1,3]anthracene molecule. A simple model of the molecule is shown in Fig. 2. A great deal of insight into the QHC approach can be gleaned from a consideration of this intramolecular half-adder gate. The first thing to note is

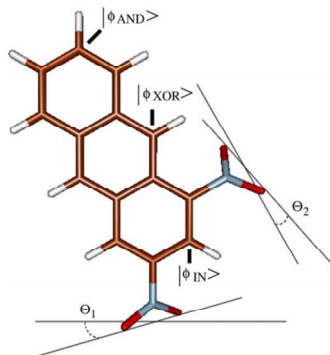


Fig. 2 > An example of a half-adder logic gate implemented using quantum Hamiltonian computing (QHC) design principles applied to a dinitro[1,3]anthracene molecule. The input bits (see truth table in Fig 3) are set by modifying the angles θ_1 and θ_2 which represent the angular orientation of the NO_2 groups with respect to the plane of the anthracene framework. A 0 is represented by an NO_2 group that is orthogonal to the molecular framework, whereas a 1 is associated with a planar NO_2 group. The locations of the carbon atoms which encode the AND and XOR outputs of the gate, and the position of the drive 'signal' (i.e. a tunnel current from a tip or an electrode), which places the molecule in a non-stationary initial state, are shown./

that the AND and XOR outputs, $|\phi_{\text{AND}}\rangle$ and $|\phi_{\text{XOR}}\rangle$ respectively, are located on two different carbon atoms. The exceptionally high spatial resolution of STM is therefore essential in order to read out the result of the calculation. The second key point is that the Hamiltonian of the system is modified via a structural distortion of the molecule – in this case, by twisting the NO_2 groups out of the plane of the anthracene backbone of the molecule. (Note that Duchemin and Joachim's study was purely theoretical. We'll come to experimental realisations of QHC very soon.)

The Hamiltonian is therefore a function of the twist angles of the NO_2 groups, and the evolution of the wavefunction of the system can be written as:

³A half-adder adds two binary digits (i.e. 0 or 1) via a combination of an XOR and an AND gate. There are therefore two outputs of a half-adder: the XOR and AND, or sum and carry, bits. The carry output is zero for all inputs other than [1,1] when it is 1. See the Boolean truth table in Fig. 3.

$$|\psi(t)\rangle = e^{-\frac{iH(\theta_1, \theta_2)t}{\hbar}} |\psi(0)\rangle \quad (2)$$

In other words, twisting the NO₂ groups modifies the angles θ_1 and θ_2 and changes the time evolution (i.e. quantum trajectory) of the system.

Having implemented a mechanism to modify the Hamiltonian of the system, the preparation of the initial state of the molecule (i.e. $|\psi(0)\rangle$) needs to be carried out. This is much more straight-forward, at least for a scanning probe microscopist⁴ than it might first appear. In order to place the molecular logic unit (in other words, the molecule) in a non-stationary initial state, an STM tip injects an electron. More accurately, the STM tip injects a series of electrons in the form of a tunnel current. Each one of the electrons comprising the tunnel current represents a separate 'preparation' event, which is followed by the time evolution of the system according to Eqn. 2.

The result of the intramolecular processing (i.e. the output of the logic gate) could also, at least in principle, be read out using an STM tip, or a very small (nanoscopic) metallic electrode. To see how this could work we'll stick with the half-adder/anthracene system. Fig. 3, again taken from Duchemin et al.'s work [9], shows how the output of the intramolecular logic can be translated to an experimental observable, namely conductance. The input bits to the gate are, as we've discussed, set by switching the conformation of the NO₂ groups (which again requires scanning probe technology). An NO₂ group that is perpendicular to the plane of the anthracene backbone encodes a 0, whereas a planar conformation represents a 1. Having defined the Hamiltonian in this way, the molecule is driven by a tunnel

current input (i.e. the drive electrode shown in Fig. 3). The truth table of the gate is then defined by the conductance (or, equivalently, resistance) of the AND and XOR output atoms, as also shown in Fig. 3.

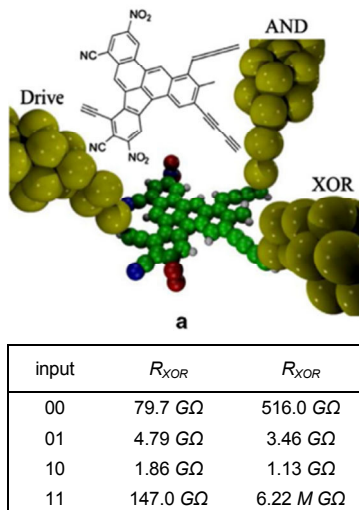


Fig. 3 > An implementation of the anthracene-based half-adder logic gate shown in Fig. 2 which uses molecular resistance (at different spatial locations) as the experimental observable which encodes the output bits. As in Fig. 2, the input bits are set by rotating the NO₂ groups either into, or 90° out of, the plane of the anthracene framework. A relatively low value of resistance encodes a 1, whereas 0 is represented by a very much higher node resistance./

The time evolution of the system (Eqn 2), is related directly to the resistance of the outputs because the tunnel currents measured at various spatial locations on the molecule – including, in particular, the output AND and XOR atoms – are directly proportional to the square of the characteristic oscillation frequencies of the evolving quantum system. In more concrete mathematical terms, the oscillation frequency, ω_{dp} between the drive (input), $|\psi_d\rangle$ and a particular output, $|\psi_p\rangle$ (where p in the case of the half-adder gate represents either the AND or the

⁴Development of QHC gate technology which does not involve the use of STM both to generate the initial non-stationary state of the system and, as described below, to read the output is exceptionally challenging. We discuss this in Section V.

XOR output), is determined by the eigenvalues of the Hamiltonian and relates to the resistance of an output node as follows,

$$\langle r | \psi_d \rangle = e^{-ikr} \quad (3)$$

For every output node, p , we have:

$$\langle r | \phi_p \rangle = T_p(E) e^{-ik_p r} \quad (4)$$

where $T_p(E)$ is the electronic transmission at a given energy for that node. If we now assume a low bias voltage (in order to consider just the transmission coefficient for states very close to the Fermi level), then the current, I_p , at node p is given by:

$$I_p = G_0 |T_p(E_f)|^2 V \quad (5)$$

Where $G_0 \left(\frac{2e^2}{h} \right)$ is the conductance quantum ($\approx 7.75 \times 10^{-5}$ S) and V is the voltage.

The key point is that each I_p is proportional to the square of the corresponding oscillation frequency, ω_{dp} , so there is a direct relationship of the measured current (or, equivalently, the resistance or conductance) at a given output node to the time evolution of the initial non-stationary/driving state, $|\psi(0)\rangle = |\psi_d\rangle$.

Although the anthracene-based half-adder design represents an important prototype for the QHC strategy, there are a couple of major issues with a practical implementation of this gate. First, co-locating three STM tips – or nanoscopic electrodes – so close to each other is, to put it mildly, exceptionally difficult (not least due to steric hindrance – the so-called “fat fingers” problem raised by Smalley in a somewhat heated debate with K. Eric Drexler a decade ago [10]). Second, the scalability of this type of design to larger molecules is problematic because the tunnel current must flow *across* the molecule (from the drive electrode to an output node), dropping exponentially with the distance between the electrodes.

To avoid these issues, Renaud and co-workers [11] proposed a rather elegant solution: simply move the drive and output nodes closer together. A logic gate which exploits this modification in the design protocol is shown in Fig. 4(a). In this case, the molecule, trinaphthylene, acts as a NOR gate. The input bits are set via modification of the Hamiltonian, as for the half-adder anthracene system of Figs. 2 and 3, but the modification of \mathbf{H} is rather more straight-forward. Instead of twisting chemical groups at the periphery of the molecule, two adsorbed atoms are translated across the surface. This type of controlled single atom translation is now routinely carried out with STM (since Eigler and co-workers pioneered scanning probe-driven atomic manipulation back in the early 90s [12, 13]), meaning that the intramolecular gate concept shown in Fig. 4(a) is much more experimentally tractable. More importantly, however, and via a clever piece of intramolecular engineering, the trinaphthylene NOR gate does not require three electrodes for input and read-out. Remarkably, one electrode is sufficient. This advance in logic gate design, by itself, means that the trinaphthylene NOR gate could be – and, as we'll see soon, was – realised, and tested, experimentally using current STM technology.

Just how is it possible to both drive and read the output of the trinaphthylene NOR gate with only a single nanoscopic electrode (i.e. an STM tip)? The basic idea is conceptually simple (although its incorporation in an intramolecular logic gate is very far from straight-forward and requires challenging design considerations): ensure that a drive channel, $|\psi_d\rangle$, is located as close as possible to an output, $|\phi_p\rangle$. This not only enables the output of the logic gate to be read out experimentally at the same position of the STM tip used for tunnel current injection – circumventing the requirement for a multi-

probe set-up – but it also neatly sidesteps the issue, discussed above, of molecular size limiting the tunnel current across the molecule. Effectively co-locating the drive and output nodes means that the size of the gate is no longer an issue – the current need flow across only a very small portion of the molecule. Despite the local nature of the current flow, however, the key point is that the input bits – i.e. the α and β atoms shown in Fig. 4 – modify the Hamiltonian of the molecule as a whole. In other words, the input data bits are “embedded” in the eigenstates of the trinaphthylene and are thus accessible (in some sense) across the entire molecular framework. In other words, while the drive and output are locally coupled, changing the inputs to the molecule has non-local consequences.

IV. Beyond Theory: Implementing Intramolecular Logic Gates

Having laid out the theoretical concepts underpinning quantum Hamiltonian computing, the key question now, of course, is just how one implements a QHC gate in practice. In particular, how is data input and read out? How experimentally demanding is it to ensure that the molecule processes the input data reliably and reproducibly? And does the theory accurately predict the behaviour of the real system?

A. Realising a QHC XOR gate

Experimental realisation of the QHC concept was achieved by Soe and co-workers in 2011 [15] (paving the way for the AtMol project). The STM images of Fig.4(b) show that the data input mechanism for the XOR gate based on a trinaphthylene molecule, schematically illustrated in the figure above (Fig. 4(a)), can indeed be implemented. Single Au atoms were pulled using the STM tip “into” the trinaphthylene molecule so as to set the α and β bits. The agreement between the

experimental STM images for the (0,0), (1,0), and (1,1) states (middle column of Fig. 4(b)) are in striking agreement with the theoretical predictions shown in the column on the right hand side of the figure (especially with regard to the relative contrast of the Au-free and Au-‘functionalised’ regions of the trinaphthylene molecule).

It’s one thing to demonstrate that the atomic/molecular manipulation required to input data to the molecule is workable, but quite another to experimentally verify the QHC concept. To do this, Soe and co-workers (including CJ) measured the differential conductance (i.e. $\frac{dI}{dV}$) of the output node of the molecule as a function of the voltage between the STM tip and the substrate (Fig. 5(a)). The features in Fig. 5 arise from different molecular orbital resonances of the molecule (namely the highest occupied molecular orbital (HOMO) (and other occupied states which are higher in energy), and the lowest unoccupied molecular orbital (LUMO)). The tunnel current at the HOMO resonance was then used as the experimental observable which codes the output state of the XOR gate.

Fig. 5(a) also highlights an important aspect of the electronic structure of an adsorbed molecule which is of key significance for QHC processing: the LUMO-related feature is not appropriate for encoding the out-put of the XOR gate in this case because of the interaction of the molecule with the underlying Au(111) substrate. There is consequently a great deal of broadening of the LUMO state of the trinaphthylene, which means that use of the LUMO in QHC data read-out is not at all appropriate: the broadening due to the surface interaction will obscure the signal due to the information processing within the molecule.

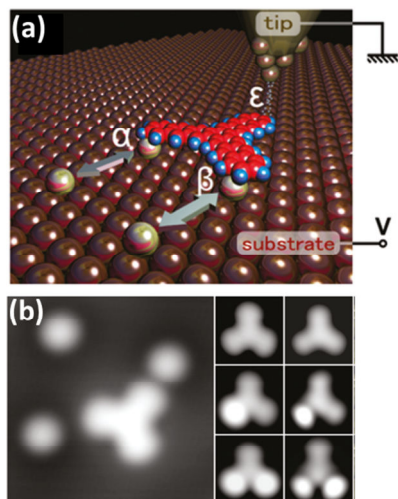
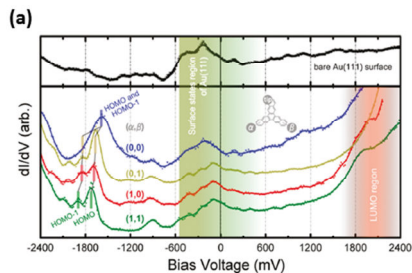


Fig. 4 > (a) A QHC XOR gate "embedded" in a trinaphthylene molecule. As for the half-adder gate of Fig. 2 and Fig. 3, the input information is fed into the gate via the manipulation of the Hamiltonian of the molecule. In this case, however, the input bits, α and β , are set by laterally translating atoms across the surface and pushing them under the legs of the molecule, rather than twisting chemical groups. This makes the trinaphthylene gate rather more tractable in a real-world experiment as compared to the half-adder, as does the use of a single tip position to both drive the intramolecular processing (by repeatedly preparing the molecule in a non-stationary state, which, like the half-adder system, evolves in time according to Eqn. 2.) and read the output. From Joachim, Renaud, and Hliwa [14]. (b) Experimental realisation of the trinaphthylene gate shown schematically in (a) above. The image on the left is an STM image of the trinaphthylene molecule surrounded by three Au adatoms, all adsorbed on a Au(111) surface. The middle column of images shows experimental STM images where first one, and then two, Au adatoms are translated as schematically illustrated in (a) above in order to set the (classical) input bits α and β . From top to bottom the input configurations are therefore (0,0), (1,0), and (1,1). The column on the right hand side of the figure shows the corresponding theoretical STM images, calculated using the elastic scattering quantum chemistry (ESQC) approach. ©Wiley-VCH Verlag GmbH & Co. KGaA, Weinheim (2012)./



(b)

(α, β)	(0,0)	(0,1)	(1,0)	(1,1)
$\bar{\alpha} \bar{\beta}$	1	0	0	0
$\Omega(\alpha, \beta) [THz]$	1.2	0.004	0.004	0.001
$I_{DB}(E_{HOMO}) [I_{T0}^*]$	1.0	0.30	0.30	0.21
$I_{DB}(E^{HOMO-1}) [I_{T0}^*]$	1.0	0.69	0.57	0.48

Fig. 5 > (a) Plot of differential conductance vs tip-sample voltage for (upper curve) a bare Au(111) surface, and (lower curves) a QHC XOR gate (based on the trinaphthylene molecule shown in Fig. 4) in its four possible input states, (0,0), (0,1), (1,0), (1,1). While the bare Au(111) surface shows a relatively featureless dI/dV spectrum away from the Fermi level (i.e. 0 volts), the trinaphthylene molecule is associated with two peaks around a voltage of ~ 6 1600 mV. These were identified by Soe et al. [15] as arising from the highest occupied molecular orbital (HOMO) and the next highest molecular orbital (HOMO-1). Note that while distinct peaks are observed for the HOMO states, the lowest unoccupied molecular orbital (LUMO) feature is broad and ill-defined due to the interaction of the molecule with the underlying Au(111) surface. For strongly interacting surfaces, this limits the "parameter space" available for QHC information processing. (b) XOR truth table for the trinaphthylene gate. The product of the NOT values of α and β , the input binary digits, are shown in the first rows. The second row is the calculated value of the Rabi oscillation frequency for the various input configurations. The bottom two rows show the calculated and measured normalised tunnel current at the HOMO resonance for each of the input bit configurations. The (0,0) configuration is associated with a higher tunnel current value than any of the other input states, thus encoding XOR gate behaviour./

A truth table based on the experimental tunnel current measurement at the HOMO level is shown in Fig.5(b). The agreement with theoretical predictions (from elastic scattering quantum chemistry (ESQC) simulations) is affected by the same type of molecule-surface interactions described above but the overall trends are sufficiently robust so as to demonstrate that the XOR logic function is present in the experimental realization of the gate.

B. Counting Atoms

Can molecules count? This question was posed, and answered, by Manzano et al. [16] in the context of data input to a coronene molecule. In this case the aim was not to implement an intramolecular logic gate. Instead, the molecule's ability to distinguish between different numbers of atoms at its 'inputs' was ascertained. Coronene was chosen because of its high symmetry – there are, in principle, six input positions for atoms (see Fig. 6). Just as for the trinaphthylene XOR gate discussed above, the atom-counting processor's in-puts were set by STM-actuated manipulation of Au adatoms, and the output was encoded in the differential conductance of the HOMO state of the molecule. For the coronene counter, however, it was not the tunnel current intensity at the HOMO level which was exploited; instead, shifts in the energy of the HOMO peak were used to determine the state of the molecule's input nodes.

Typical differential conductance spectra for the HOMO state of the coronene, before and after the addition of a Au atom to the molecule, are shown in Fig.6(a). The figure also includes spatial maps of the differential conductance of the HOMO state, as measured experimentally and as calculated via ESQC simulations. The addition of a Au atom not only modifies the energy of the HOMO level – as clearly seen in the spectra of Fig. 6(a) – but the overall symmetry and spatial distribution

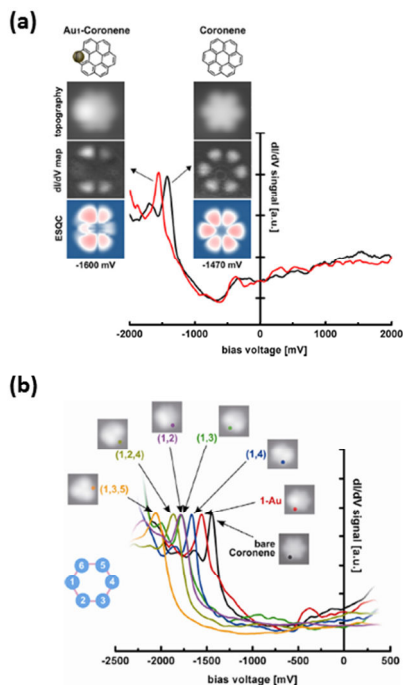


Fig. 6 > An atom counter based on a coronene molecule. **(a)** In the insets the structure of the coronene molecule, both with and without an attached Au atom, is shown alongside a corresponding STM image; an experimental dI/dV map of the HOMO state of the molecule; and the spatial distribution of the HOMO differential conductance as simulated by the ESQC technique. The graph shows the shift in the HOMO-related peak in the differential conductance (or, equivalently, the density of states of the molecule) on addition of a Au atom. Note that both the energy and spatial distribution of the HOMO are affected by the bonding of the molecule to the Au atom. **(b)** Changes in the position of the HOMO-derived peak in the experimental dI/dV curves measured at various points on the coronene molecule (as indicated by the variously coloured dots). The shift in the HOMO energy is linear with the number of added atoms (not shown) and is approximately 550 meV/atom./

of the HOMO state changes. As Manzano et al. point out, this spatial modification of the HOMO state must be taken into account in the atom counting protocol.

In Fig. 6(b), the coronene molecule has been 'loaded' with different numbers of Au atoms resulting in a variety of shifts in the energy of the HOMO state. These energy shifts turn out to be linear with respect to the number of Au atoms, with a shift of approximately 550 meV for each added gold atom. However, the choice of spatial position within the molecule at which to measure the HOMO energy, and the sequence/nodes chosen for the addition of Au atoms are both key aspects of the counting protocol. When these limiting provisos are taken into account then the coronene molecule indeed can be said to count atoms – it “converts” (in some sense) its input state to the shift in energy of a molecular orbital. This type of protocol, however, cannot work with any arbitrary molecule. In order to encode the input state in the shift of the HOMO level, it is essential that the highest occupied molecular orbital is delocalized over the entire molecule.

V. But do we Need Molecules? Dangling Bond Logic

A fascinating question now arises. Do we really need to use molecules for QHC? After all, what is required is 'just' a quantum state whose Hamiltonian can be tuned using appropriate inputs, and a means of translating the quantum output to a classical observable such as tunnel current. Molecules certainly fulfil these requirements, but so too – in principle – does any system which is capable of supporting interacting and modifiable orbitals. Indeed, one might argue that the ideal system would be at substrate where patterns of orbitals could be created from a “blueprint”, enabling the generation of QHC gates without the need to do complicated synthetic chemistry.

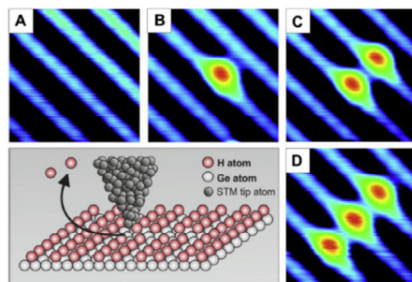


Fig. 7 > “Dialling up” a QHC logic gate - generation of single dangling bonds using an STM. The schematic shows how an STM tip can be used to extract single atoms from either a H:Si(100) or a H:Ge(100) surface, where the “H:” nomenclature indicates hydrogen termination. The tip injects tunnelling electrons which vibrationally heat the surface and lead to the desorption of hydrogen atoms. This exposes a silicon atom, and its associated unsaturated dangling bond, to the vacuum. Figures (A)-(D) are STM images of a clean H:Ge(100) surface, and the same surface region following the removal of one, two, and then three hydrogen atoms respectively. The removal of a H atom leads to a much higher density of states at the position of the silicon dangling bond and this in turn produces an intense contrast maximum in the STM image./

Luckily, such a system exists. Si(100) and Ge(100) surfaces⁵ can be readily passivated using atomic hydrogen. The hydrogen saturates the otherwise reactive dangling bonds, leading to a passivated and remarkably inert surface. The benefit of the passivation for the generation of QHC logic gates is clear from Fig.7. As pioneered by Lyding et al. [17] back in the mid-nineties, an STM tip can be used to locally remove hydrogen *all the way down to the single dangling bond limit*. A flow of tunnelling electrons (with an appropriate energy) is injected into the surface above

⁵The (100) nomenclature represents the Miller indices for the crystal plane. Silicon and germanium both have a diamond-type unit cell (i.e. two inter-penetrating *face-centred cubic* lattices). The (100) plane represents a face of that unit cell and, in the absence of any type of surface reconstruction (i.e. the movement of atoms in order to lower the surface free energy), has a square symmetry. As we'll see, however, surface reconstruction is an incredibly important issue in the context of QHC architecture based on dangling bonds.

a hydrogen atom. This leads to vibrational heating of the Si-H bond, increasing its energy in increments of vibrational quanta up until the point where the H atom can dissociate from the silicon and desorb (as sketched schematically in Fig.7). This means that single dangling bonds (i.e. individual electron orbitals) can be placed on the surface in a pre-defined pattern. Three dangling-bond-generation events are shown in Fig. 7.

The relative positions and interactions of the dangling bonds determines the conductance of the structure created by STM-actuated extraction of H atoms. The DB assembly can be thought of as an artificial molecule and, indeed, Schofield et al. [18] have shown the emergence of molecular orbital states when neighbouring DBs couple to each other. Thus, the strategies discussed above in the context of intramolecular computing can be extended to DB arrangements at passivated silicon and germanium surfaces, with the key difference that logic gates can be “written” with the STM tip, rather than being embedded in a molecule via (possibly extremely challenging) synthetic chemistry.

In the molecular QHC gates discussed thus far, data input was via the addition of atoms to the molecule in question. A similar strategy is used for H:Si-based gates, where the presence or absence of hydrogen is used to set the input bits. The experimental observable used to determine the output of the gate is again tunnel current (or tunnel conductance). Examples of simple Boolean logic operations implemented using DB computing are shown in Fig. 8. In this case, current flows through the structure in a similar manner to the anthracene gate set-up shown in Figs. 2 and 3¹. In each

case in Fig. 8, the addition of H atoms to passivate Si DBs modifies the current flow through the dangling bond assembly.

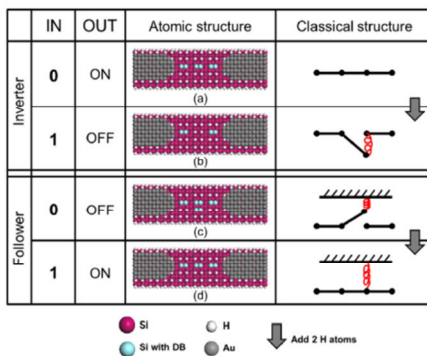
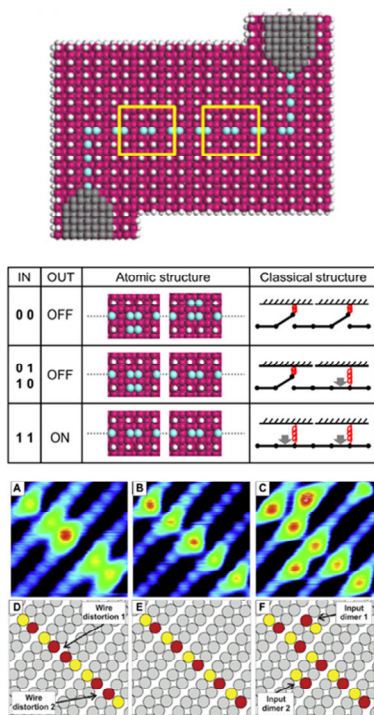


Fig. 8 > Examples of basic Boolean operations implemented by the interactions of dangling bonds (DBs) on a hydrogen-passivated silicon (or germanium) surface. The output is encoded in the current wing between the nanoscopic contacts represented by the grey pads. The input state is set by the absence or presence of hydrogen atoms. In the inverter gate, the conductance through the DB array is strongly affected by repassivating the central two silicon atoms: the presence of H atoms (logic: 1) leads to a low conductance (OFF), whereas the absence of H (logic: 0), i.e. the presence of a DB, produces a higher conductance (ON). Thus, an inverter is encoded. In the lower half of the figure the same type of strategy is used to encode follower behaviour. The additional depassivated silicon atoms (as compared to the arrangement in the top row of the diagram) introduce electronic states which modify the conductance of the DB assembly. Repassivating those atoms (lowest row) increases the conductance, yielding a “1” output state./

This strategy can be extended to encode logic gates. Fig. 9 shows how an AND gate would be implemented in DB-based QHC. Again, the presence of hydrogen is used to encode a logical “1”, while unpassivated silicon atoms represent a “0” state. Instead of lateral atom translation, as was the case for the intramolecular logic gates based on triphenylene and coronene, the inputs to the DB gates are set via what is usually called vertical atom manipulation - in this case the extraction

¹Note, however, that the requirement for nanoscopic electrodes can be circumvented and a single STM tip can be used for data read-out in an analogous fashion to the intramolecular XOR and atom-counter processors described above [19].



or deposition of hydrogen using a scanning probe. Kolmer et al. [19] have experimentally shown that DB gates and input bits can be generated using STM extraction of hydrogen (see Fig. 9).

But there's a significant difference between the structure of the DBs shown in the schematic at the top of Fig. 9 and their "real world" counterparts: the depassivated dimers do not remain planar as in the schematic (and associated theory). Instead, the ground state of a hydrogen-free dimer (on either the Si(100) or Ge(100) surface) is a buckled geometry, where one atom moves into the surface and the other moves out of the plane (as shown in Fig. 10). We'll discuss the implications of this for DB logic soon, but first let's focus on the extent to which the DB gate generation process can be automated (and thus brought closer to the types of lithography

Fig. 9 > Implementation of an AND gate using DB logic. **Top:** Schematic illustration of the DB arrangement which encodes AND functionality. As shown in the truth table directly below the illustration, the input bits to the gate are once again set using the presence or absence of H atoms. A "0" input is coded by the presence of DBs (shown as the blue circles), while a "1" state is set by passivating those DBs with hydrogen atoms. The interactions of the DB orbitals strongly modify the electronic density of states within an energy range of a few volts around the Fermi level. This in turn modifies the conductance of the DB assembly, which encodes the output state of the gate. **Bottom:** (A)-(C) Experimental demonstration of the creation of DB arrangements via STM-driven hydrogen atom extraction from the H:Ge(100) surface, with accompanying schematic models shown in (D)-(F). Here grey circles represent the hydrogenated germanium atoms while red and yellow circles illustrate the "up" and "down" atoms of the buckled dehydrogenated dimers. The buckling arises from a Jahn-Teller-like distortion of the Ge dimer unit due to a degeneracy of the electronic states at the Fermi level for a planar dimer; buckling (where the dimer distorts so that one atom moves out of the surface plane, while the other moves "down") removes this degeneracy and opens up a gap around the Fermi level (see Fig. 10). Buckling is not taken into consideration in the schematic model shown at the top of the figure./

and fabrication protocols which are the bedrock of the micro- and nanoelectronics industries). In other words, is it possible to remove the human operator and have the scanning probe system autonomously generate DB gates?

VI. Following the Blueprint

The probe of an STM (or AFM) is simultaneously an exceptionally powerful tool for the imaging, manipulation, and spectroscopic probing of matter at the atomic and (sub)molecular levels, and the bane of every scanning probe microscopist's working life. A very large fraction of an SPM user's day can be spent on coercing the tip into giving not only atomic resolution but, increasingly, a specific type of imaging state due to a perhaps rare and difficult-to-achieve state of the apex of the probe. This is almost invariably carried out through a process of

trial-and-error by scanning probe microscopists. Various strategies – including voltage pulsing, gentle (and not-so-gentle) crashing into the sample surface, and high current imaging, or a combination of all three – are used to force the apex of the tip into a particular structure which yields the type of resolution the operator requires.

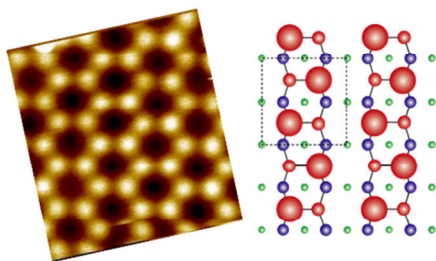


Fig. 10 > Non-contact atomic force microscopy image of the clean Si(100) surface (i.e. without hydrogen passivation) at 5 K with the corresponding structural model shown on the right. In the model large circles represent atoms that have moved out of the surface plane, whereas small circles are used to illustrate atoms that have moved “into” the plane. This buckling effect is very clearly visible in the NC-AFM image, where zig-zag rows of silicon atoms are observed. Unlike STM, NC-AFM is sensitive to the local chemical reactivity of the surface, rather than the density of states. Thus, there tends to be a much greater correlation of an NC-AFM image with the atomic structure of a surface than is often the case with STM./

But it doesn't have to be like this. In principle, the computer system at the heart of the SPM instrument is capable of not only autonomously identifying when atomic resolution has been achieved but, via image analysis, categorisation, and segregation algorithms, it could also coerce the tip into a given state. Having then achieved that tip state the SPM system could fabricate a DB gate from a pre-defined blueprint, checking after each dangling bond generation event that the hydrogen extraction had been successful and that the imaging process had not been affected. (And if the imaging resolution *had*

changed, the system could restore the tip state accordingly.)

In principle. In practice, this is an exceptionally challenging process to automate. The human eye is exceptionally good – sometimes too good – at analyzing images and extracting patterns. Developing algorithms which mimic and automate the abilities (and scientific “intuition”) of a human operator is, as we have found, far from straight-forward. Nonetheless, protocols and algorithms have been developed (during the course of the AtMol project) which enable the autonomous acquisition of atomic resolution images from an initial tip state which yielded only noisy images devoid of any atomic structure, or indeed any type of reproducible feature at all.

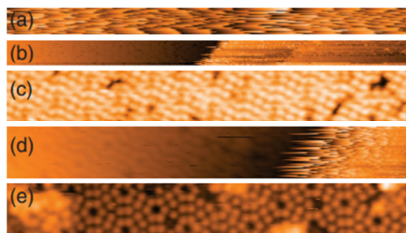


Fig. 11 > Automated optimisation of an STM image. The initial state of the tip was deliberately chosen to be as poor as possible (by pushing the apex of the probe into a graphite sample and dragging it across the surface). (a) The first image of the Si(111)-(7x7) surface taken. (b)-(e) show variations in the quality of the imaging induced by the automatic optimisation strategy (implemented on an Omicron Variable Temperature STM system). From Stirling et al. [21]. ©American Institute of Physics (2013)./

The output of this automated tip optimisation protocol (ATOP) is shown in Fig. 11 for a Si(111)-(7x7) sample where the probe was first crashed into, and dragged across, a graphite surface to ensure that its initial state was far away

²See Stirling et al. [20] and references therein for a discussion of false pattern recognition and the associated psychological biases in image interpretation.

from the tip structure required to attain atomic resolution. A variety of different image analysis metrics (which are now available as part of the SPIW package [21]) were used in concert with tip modification techniques in order to coerce the probe into providing atomic resolution images. In parallel with the development of the ATOP routines, protocols for the automated identification of hydrogen extraction events (using the tunnel current-driven vibrational heating described above) were developed and embedded within the (commercial) software used to control an ultrahigh vacuum STM. Essentially arbitrary patterns of DBs (Fig. 12) can be generated via a template of (x,y) coordinates passed to the routine.

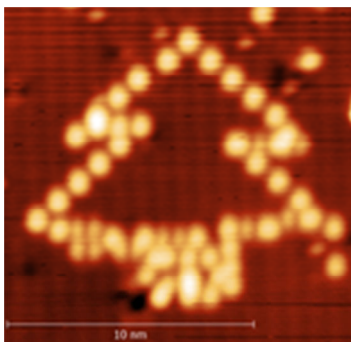


Fig. 12 > User-defined pattern of DBs created by an automated hydrogen extraction algorithm. The DBs were created one at a time. At each (x,y) coordinate, the sample bias is slowly ramped while the tip remains under feedback control. Both the absolute z height and the local gradient of $z(V)$ are continuously measured and the success of a hydrogen extraction attempt is determined by the variation of these quantities. We find that this approach to depassivation results in considerably fewer tip change events./

VII. Bit by Bit

The creation of DB patterns and assemblies of the level of complexity required for logic gate implementation is, therefore, achievable. This can happen either “by hand” (i.e. where a human

operator painstakingly directs the probe to the desired position and initiates the hydrogen extraction at each point) or via automated methods as described in the preceding section (where the probe microscopist is surplus to requirements, at least in terms of fabricating the structure). But two key problems remain. The first of these is the dimer buckling issue described above - we'll come back to that in the next section. Here we'll discuss the key hurdle that must be surmounted in order to input data to the type of DB gate shown in Fig. 9: just how do we deposit single H atoms with atomic precision on the surface so as to set the input bits? Extraction of hydrogen can be achieved via tunnel current injection, but how do we (re-)passivate a DB?

Only scanning probe microscopes have the atomic precision needed to restore hydrogen at the specific locations required to ensure that the input bits to a DB gate are set appropriately. One route to locally hydrogenating a DB (or, indeed, a nanoscopic region of the clean silicon(100) surface) was studied by Labidi and co-workers [22], who leaked in molecular (i.e. unactivated) hydrogen, which does not react with the silicon dimers, and locally converted it to atomic hydrogen (again via tunnel current excitation) to passivate DBs. (See Figs. 13 (a)-(d)). While in principle this approach *could* be used to repassivate DBs and so (re)set the input bits of DB logic gates, it would be an exceptionally time consuming strategy. The molecular hydrogen surrounding the STM would have to be pumped away during the tip-induced depassivation phase, otherwise it could get 'cracked' and end up passivating the DB created by the tip. The need to repeatedly leak in and then pump out hydrogen would set the operating bandwidth of the gate not at the GHz level of conventional processors, but in the range of tens of milli-Hz at best.

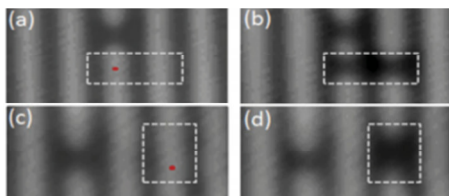


Fig. 13 > Hydrogen passivation of dimers on the clean Si(100) surface by “cracking” H₂ to atomic hydrogen using an STM tip. The red dots in (a) and (c) show the position at which a voltage pulse was applied to the tip. The images taken directly afterwards, (b) and (d) respectively, show a dramatic reduction in the density of states at the tip position which was interpreted as arising from H-passivation of the dimer. From Labidi et al. [22]. ©American Physical Society (2011)./

So how else might it be possible to re-passivate a dimer? Could hydrogen be transferred from the tip to a DB simply by pushing the tip into the surface; in other words, is (mechano)chemical force enough to drive the exchange of a H atom? A series of density functional theory (DFT) calculations was used, along-side a set of NC-AFM experiments, to explore just this possibility. It turns out that, as is generally the case with any scanning probe technique, the tip apex plays a crucial role in enabling, or prohibiting, the extraction of hydrogen. On the face of it, this is not a very surprising result. Nonetheless, the extent to which the tip state influences the H deposition process makes experimental realisation of a single DB (re)passivation process even more challenging than it might appear at first glance. With STM, it's essential to have an atomically sharp tip in order to generate an atomic resolution image. With NC-AFM, however, the bar is raised still further: the image not only depends critically on the precise structure (down to the type of dangling bond orbital(s)) at the end of the tip, but even the back-bonding of the terminating atom to its neighbours in the apex of the probe can play a role.

Similarly, while it's possible to desorb H atoms using tunnelling current injection from a variety of different tip states, atomic manipulation with NC-AFM is even more critically dependent on the precise structure of the tip cluster than is the case for NC-AFM imaging. Fig. 14(a) shows a set of different NC-AFM images of the H:Si(100) surface acquired with a variety of different tip states on different days. Note how in each case the dimers appear as depressions, rather than as raised features. Ninety per cent of our NC-AFM images of H:Si(100) show this contrast inversion and, for the reasons discussed by Sharp et al. [23], this arises because the tip is hydrogen-passivated and thus has effectively no direct chemical interaction with the H:Si(100) surface. In other words, the depth of the potential energy well associated with the tip-sample interaction is exceptionally small.

Having a hydrogen-passivated tip apex is an advantage in the context of transferring a H atom to a DB – half the work is done already. But we find that, despite the apex being H-terminated, it has not been possible (to date) to re-passivate a DB using mechanochemical force in a NC-AFM experiment. The results of the DFT calculations shown in Fig. 14 provide key insights into just why it's so difficult to transfer a hydrogen atom from the tip to the surface. Figs. 14(b) and (c) show two “archetypical” tip structures - a so-called “H3” tip (so called because of the way the terminating silicon atom is back-bonded to its neighbours; the nomenclature comes from the Si(111) surface science literature) and a dimer-terminated tip, respectively. (The charge density in a 1eV window below the Fermi level is superimposed on the ball-and-stick model in each case so as to aid visualisation of the dangling bond shape and symmetry).

What happens if we hydrogen-terminate each of the tips shown in Fig. 14(b) and (c) and then attempt to passivate a dangling

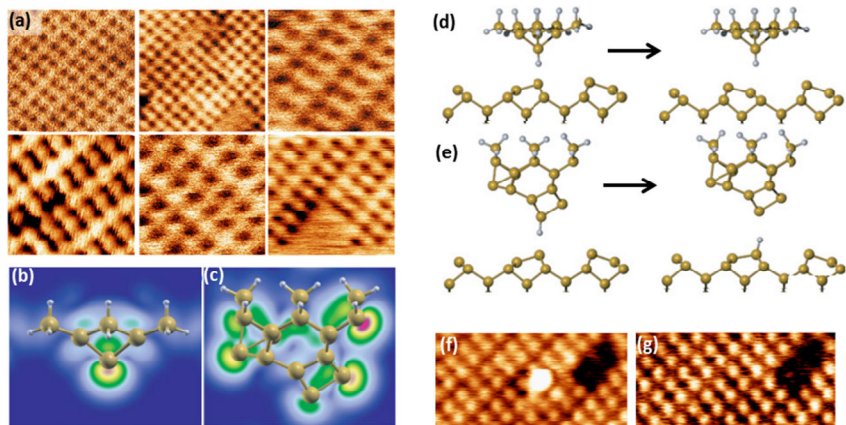


Fig. 14 > Extracting and depositing hydrogen using a scanning probe: the importance of the tip apex. **(a)** A set of NC-AFM images of the H:Si(100) surface showing H-passivated dimers as depressions, rather than protrusions. This type of imaging mode occurs ~90% of the time in our experience and is a signature of a H-passivated tip. **(b), (c)** Ball-and-stick models of two types of tip – a H₃-, and a dimer termination, respectively. The charge density in a 1 eV window below the Fermi level (plotted on a log scale) has been superimposed to highlight the spatial distribution and orientation of the dangling bond(s) at the apex of the tip. **(d)** Snapshots taken from DFT calculations of the structure of the tip (and surface) on approach, and retraction, from the dangling bond of the underlying dimer. Note that the H atom remains on the tip despite the applied force being sufficient to flip the dimer. **(e)** With a dimer tip apex, however, the hydrogen atom is transferred to the surface. **(f)** A H:Si(100) surface with a tip-generated DB at the centre of the image. (STM scan). **(g)** In the subsequent STM image the DB has disappeared due, we believe, to the transfer of a H atom from the tip. From Jarvis et al. [24]. ©American Physical Society (2012)./

bond at the surface? Snapshots of the DFT simulations of the tip-sample interaction are shown in Figs. 14(d) and (e). (Note that these are not schematic illustrations - they are the direct output of the DFT calculations.) In Fig. 14(h) a hydrogen-terminated H₃ tip approaches the “up” atom of a dimer directly underneath. The tip is pushed into the surface DB up to the point where the dimer flips due to the mechanochemical force. At no point, however, does the H atom transfer to the surface. It remains on the tip.

But if, as in Fig. 14(e), a dimerised tip is used, the H atom transfer is possible. As Jarvis et al. [24] discuss, the propensity for the dimerised tip to let go of its terminating hydrogen atom is easily understood from a simple calculation of the energy balance as the tip approaches the surface or, equivalently, from a consideration of the

reactivity of the particular tip apex (i.e. Fig. 14(b) or (c)) with a hydrogen atom, as compared to the H-Si(100) binding energy.

We have not yet achieved transfer of a H atom from a NC-AFM tip to a Si(100) surface - due, most likely, to our inability to create or access⁸ the appropriate structure of the tip apex. However, on rare occasions we *have* observed repassivation while scanning over a DB created previously by the STM tip. This is also shown in Fig. 14, where the DB visible in the centre of Fig. 14(f) disappears in a subsequent scan, Fig. 14(g). As the imaging was carried out at 77K, and the diffusion barrier for DB motion along the dimer rows of a

⁸Our NC-AFM experiments to date have been carried out at 77 K or 5 K. We speculate that it may be that the types of tip state that form at those temperatures are kinetically hindered from reaching structures which are compatible with transfer of hydrogen to the Si(100) surface.

H:Si(100) surface is ~ 1.2 eV, the natural hopping rate can be estimated as 10^{52} Hz. The disappearance of the DB is thus not related to it diffusing out of the scan window, and we attribute its absence in Fig. 14(g) to repassivation by a H atom from the STM tip.

VIII. Mind the Gap

Although the experimental challenges associated with the fabrication and actuation of DB logic gates are, as we've seen, complicated and multi-faceted, there is clear scope – if the H “repassivation” issue can be addressed – for the protocols and, ultimately, the technology to be pushed considerably further. Moreover, a

“hybrid” strategy involving a combination of DB circuitry with intramolecular QHC has particularly exciting potential for radically new forms of information processing. The intramolecular component of that hybrid technology could involve the types of gates discussed in previous sections or, as has been explored by Koch et al. [26] graphene nanoribbons of the type shown in Fig. 15. The nanoribbon conductance depends critically on its atomic structure and geometry (particularly the extent of bending), opening up particularly intriguing new avenues of research involving mechanically actuated logic gates and information processing.

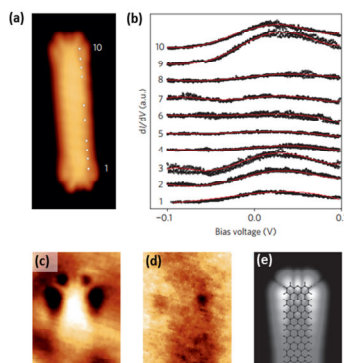


Fig. 15 > The electronic structure of a graphene nanoribbon. **(a)** STM image of the nanoribbon; **(b)** dI/dV spectra acquired at the various points highlighted in (a). Note the presence of a state crossing the Fermi level (0 V) at the ends of the ribbon. This is a localised Tamm state; **(c)** dI/dV map acquired at a bias voltage of 50 mV showing the localized spatial distribution of the Tamm state; **(d)** dI/dV map acquired for a voltage of -550 mV for comparison; **(e)** Calculated conductance map at 50 mV (simulated using ESQC theory). From Koch et al. [26]. ©Nature Publishing Group (2012)./

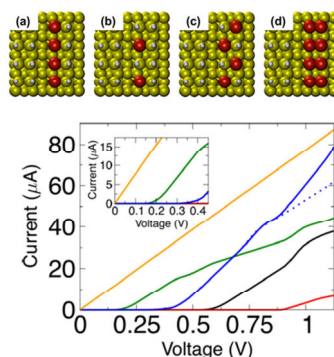


Fig. 16 > Schematic models of different dangling bond arrangements at the H:Si(100) surface. The structure shown in **(a)** is unstable against an instability which drives the dimers to buckle away from a planar state. This is accompanied by strong electron correlations which open up a gap in the density of states of the DB assembly, thus adversely affecting its conductance. The structures shown in **(b) - (d)** were theoretically assessed as to their electronic (and electrical transport) properties. The lower half of the figure shows IV curves of the single-row DB wire (black), the half-row (i.e. structure (b)) (red), zigzag (green), and dimer row (blue) dangling-bond wires. The yellow line is a “control” and represents the IV characteristic of a one-channel metallic wire, such as a monatomic gold wire. From Kepenekian et al. [25]. © American Chemical Society (2013)./

However, we now need to return to the issue of dimer buckling which we set aside in the last section. Buckling has exceptionally important implications for the electronic structure of any type of dangling bond system (bit, wire, or gate) because, as we've noted before, it opens up a gap in the electronic structure. This substantially lowers the conductance of the DB system. Recognising this, Kepenekian et al. considered a number of band engineering strategies to circumvent the detrimental effects arising from buckling. They focussed, in particular, on enabling a greater extension of the electronic states so as to reduce electronic correlations and, thus, to improve the conductance of the DB system. They examined three different arrangements of DBs, as shown in Fig. 16, and found that both the zig-zag arrangement and the row of depassivated dimers (i.e. a row of neighbouring DBs) substantially reduced electron correlation and thus the electronic conductance improved. However, the depassivated dimer row is coupled more strongly to the underlying bulk substrate which gives rise to problems with leakage current. Hence, the zig-zag arrangement of Fig. 16(c) represents the best compromise.

IX. Making Contact

So all of the components required for information processing via the QHC strategy are in place: intramolecular information processing; dangling bond gates and wires; a mechanism of setting and resetting input bits (albeit based on scanning probe technology); and protocols to read out the output of the logic operation. And yet, to use a clichéd expression beloved of politicians in the UK, thus far we've ignored the elephant in the room. Just how could these apparently

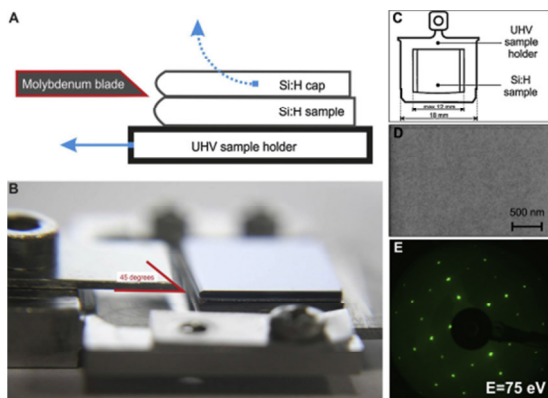


Fig. 17 > The strategy used to cap, transfer, and uncap hydrogen-passivated Si(100) samples from one ultrahigh vacuum system to another. **(A)** shows the mechanical “cleavage” strategy used to remove the cap; **(B)** a photograph of the debonder; **(C)** dimensions of sample and holder; **(D)** a scanning electron microscopy image of the H:Si(100) surface following debonding; **(E)** a low energy electron diffraction (LEED) pattern from the debonded sample. From Kolmer et al. [19] ©Elsevier (2014)./

esoteric and very delicate surface-supported systems be connected to the macroscopic “real world”, i.e. integrated with current device technology?

A major element of the AtMol project was a drive to attempt to integrate the type of atomic scale engineering we've discussed throughout this article with traditional silicon micro-/nanoelectronics. The first step in this exceptionally challenging goal is to ensure that hydrogen-passivated surfaces created in a microelectronics facility can be capped and transferred out of vacuum from one system to another. In a *tour de force* experimental programme, three teams of researchers from Jagiellonian University (Krakow), CEA-LETI (Grenoble), and CEMES-CNRS (Toulouse) developed a strategy to enable just this type of inter-UHV system transfer, with the H:Si(100) sample being capped before exposure to air and subsequently

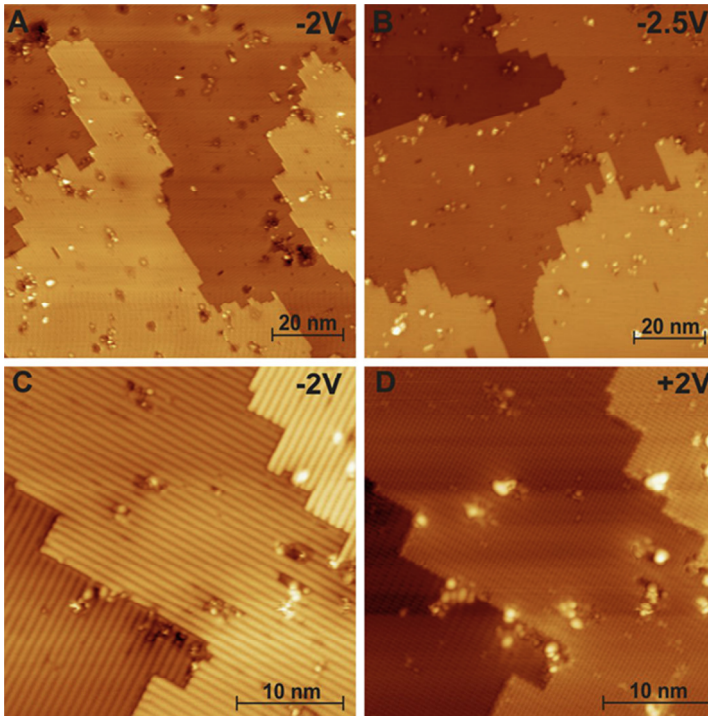


Fig. 18 > STM images of the surface of the debonded H:Si(100) sample. Large defect free regions are visible. From Kolmer et al. [19] ©Elsevier (2014)./

decapped when it was placed in the second UHV system [19]. The decapping strategy is shown in Fig. 17. It relies on van der Waals bonding between the H:Si(100) surface and the capping wafer, meaning that the cap can be removed by simple mechanical force.

The quality of the sample surface following decapping is best ascertained by scanning probe microscopy and, as shown in Fig. 18, it rivals the quality of many H:Si(100) samples which are prepared *in situ*. The defect density is certainly sufficiently low such that extended DB patterns can be created, as clearly, and impressively, shown in Fig. 19.

Where now for QHC and DB technology?

The results shown in Figs. 17 -19 indicate that integration with silicon microelectronics is entirely feasible from the perspective of preserving the atomic-scale integrity of the surface. The next step in the evolution of QHC is clear: a DB or intramolecular QHC gate on a H:Si(100) (or H:Ge(100)) surface needs to be fabricated, capped with a suitably microstructured cavity fabricated in the capping wafer, and transferred to another system for measurements (or, indeed, additional modification). There then remains the immensely challenging task of connecting the DB and/or (intra)molecular circuitry to macroscopic contacts. The legacy of the AtMol project is that it has established the

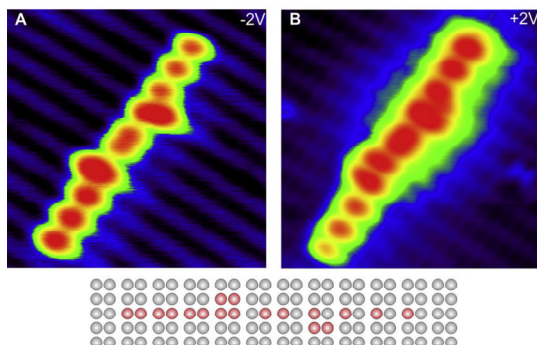


Fig. 19 > Filled and empty state images of an extended DB pattern created by STM-induced DB creation on a debonded H:Si(100) sample. The schematic diagram below the images shows the arrangement of the DBs./

protocols and methods required – and the pitfalls to avoid – for the continuing development of next-generation, and sub-molecular, information processing.

References

- [1] A. Aviram and M. Ratner, *Chem. Physics. Lett.* 29, 277 (1974).
- [2] C. Joachim, J. Gimzewski, and A. Aviram, *Nature* 408, 541 (2000).
- [3] J. Fiurasek, N. Cerf, I. Duchemin, and C. Joachim, *Physica E* 24, 161 (2004).
- [4] C. Joachim, *Nature Nanotech.* 7, 620 (2012).
- [5] H. Vazquez, R. Skouta, S. Schneebeli, M. Kamenetska, R. Breslow, L. Venkataraman, and M. S. Hybertsen, *Nature Nanotech.* 7, 663 (2012).
- [6] B. P. Lanyon, M. Barbieri, M. P. Almeida, and A. G. White, *Phys. Rev. Lett.* 101, 200501 (2008).
- [7] K. C. Lee, M. R. Sprague, B. J. Sussman, J. Nunn, N. K. Langford, X. M. Jin, T. Champion, P. Michelberger, K. F. Reim, D. England, et al., *Science* 334, 1253 (2011).
- [8] I. Duchemin and C. Joachim, *Chem. Phys. Lett.* 406, 167 (2005).
- [9] I. Duchemin, N. Renaud, and C. Joachim, *Chem. Phys. Lett.* 452, 269 (2008).
- [10] K. Drexler, *Chem. Eng. News.* 82, 4 (2004).
- [11] N. Renaud, M. Ito, W. Shangguan, M. Saeys, M. Hliwa, and C. Joachim, *Chem. Phys. Lett.* 472, 74 (2009).
- [12] D. Eigler and E. Schweizer, *Nature* 344, 524 (1990).
- [13] M. Crommie, C. Lutz, and D. Eigler, *Science* 262, 218 (1993).
- [14] C. Joachim, N. Renaud, and M. Hliwa, *Adv. Mater.* 24, 312 (2012).
- [15] W.-H. Soe, C. Manzano, N. Renaud, P. de Mendoza, A. De Sarkar, F. Ample, M. Hliwa, A. M. Echavarren, N. Chandrasekhar, and C. Joachim, *ACS Nano* 5, 1436 (2011).
- [16] C. Manzano, W. H. Soe, M. Hliwa, M. Grisolia, H. S. Wong, and C. Joachim, *Chem. Phys. Lett.* 587, 35 (2013).
- [17] T. Shen, C. Wang, G. Abeln, J. Tucker, J. Lyding, P. Avouris, and R. Walkup, *Science* 268, 1590 (1995).
- [18] S. R. Schofield, P. Studer, C. F. Hirjibehedin, N. J. Curson, G. Aeppli, and D. R. Bowler, *Nature Comm.* 4, 1649 (2013).
- [19] M. Kolmer, S. Godlewski, R. Zuzak, M. Wojtaszek, C. Rauer, A. Thuair, J.-M. Hartmann, H. Moriceau, C. Joachim, and M. Szymanski, *Appl. Surf. Sci.* 288, 83 (2014).
- [20] J. Stirling, I. Lekkas, A. Sweetman, P. Djuranovic, Q. Guo, B. Pauw, J. Granwehr, R. Levy, and P. Moriarty, *PLOS ONE* 9, e108482 (2014).
- [21] J. Stirling, R. A. J. Woolley, and P. Moriarty, *Rev. Sci. Instr.* 84, 113701 (2013).
- [22] H. Labidi, L. Kantorovich, and D. Riedel, *Phys. Rev. B* 86, 165441 (2012).
- [23] P. Sharp, S. Jarvis, R. Woolley, A. Sweetman, L. Kantorovich, C. Pakes, and P. Moriarty, *Appl. Phys. Lett.* 100, 233120 (2012).
- [24] S. Jarvis, A. Sweetman, J. Bamidele, L. Kantorovich, and P. Moriarty, *Phys. Rev. B* 85, 235305 (2012), ISSN 1098-0121.
- [25] M. Kepenekian, R. Robles, C. Joachim, and N. Lorente, *Nano Lett* 13, 1192 (2013).
- [26] M. Koch, F. Ample, C. Joachim, and L. Grill, *Nature Nanotech.* 7, 713 (2012).

C /Simancas 21, Madrid

www.dayfisa.com

Tlf.: 91 315 40 41

dayfisa@dayfisa.com



DAYFISA

Desarrollo, Asesoría y
Formación Informática S.A.



GRUPO DAYFISA



Servicios informáticos integrales ❧
Integral IT Services

Diseño y desarrollo de software ❧
Software design and development

Consultoría y outsourcing ❧
Consulting and outsourcing

Servicio técnico y mantenimiento ❧
Technical service and maintenance

Venta de material informático ❧
Computer equipment sales

Departamento de formación ❧
Training department

InforTel
COMUNICACIONES

Infortel Comunicaciones S.L.

C /Simancas 21, Madrid

www.infortel.es

Tlf.: 91 314 03 53

infortel@infortel.es



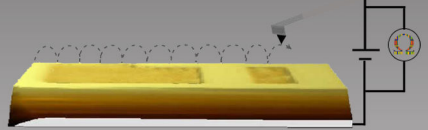
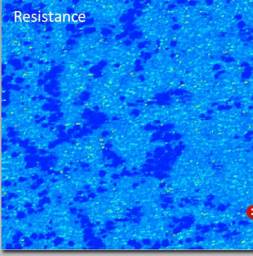
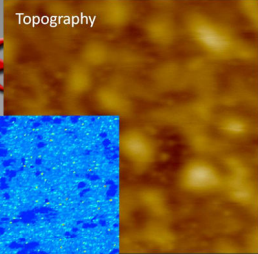
Scientec

SURFACE ANALYSIS

Quantitative Electrical measurements with intermittent contact on soft material

Innovative & Unique

CSI Concept Scientific Instruments



- Soft material
- No friction
- Quantitative measurements over 10 Decades

PH3T, Organic Solar Cell

Soft ResiScope

AFM Nano-Observer

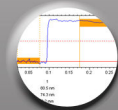
ResiScope II



- Flexible and powerful
- True Single-Pass KFM
- Multiple Environnements (Gas & temperature control, liquids...)
- High resolution & Low noise system

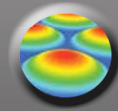
Quantitative resistance and current measurements (10 Orders of magnitude)

2D-3D MECHANICAL PROFIOMETRY



3D OPTICAL SURFACE PROFIOMETRY

Interferometry (PSI/VSI), Confocal, Digital holography...



AND ALSO NANO-INDENTATION



Contact us at +33 (0)1 64 53 27 00 Info@scientec.fr - www.scientec.fr